AD-A136826
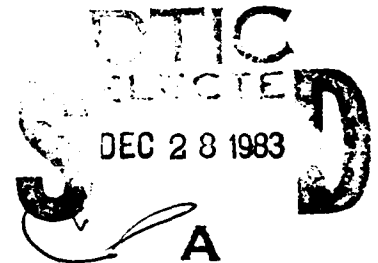
TECHNICAL REPORT ARBRL-TR-02535

NUMERICAL INVESTIGATION OF THE AERODYNAMICS
AND STABILITY OF A FLARED AFTERBODY FOR
AXISYMMETRIC PROJECTILES AT
SUPERSONIC SPEEDS

Michael J. Nusca

DTIC
ELECTE
DEC 28 1983

A

December 1983

US ARMY ARMAMENT RESEARCH AND DEVELOPMENT CENTER
BALLISTIC RESEARCH LABORATORY
ABERDEEN PROVING GROUND, MARYLAND

DTIC FILE COPY

Destroy this report when it is no longer needed.
Do not return it to the originator.

REPORT DOCUMENTATION PAGE	READ INSTRUCTIONS BEFORE COMPLETING FORM

1. REPORT NUMBER	2. GOVT ACCESSION NO.	3. RECIPIENT'S CATALOG NUMBER
TECHNICAL REPORT ARBRL-TR-02535	AD-A136 826	

4. TITLE *(and Subtitle)*	5. TYPE OF REPORT & PERIOD COVERED
NUMERICAL INVESTIGATION OF THE AERODYNAMICS AND STABILITY OF A FLARED AFTERBODY FOR AXISYMMETRIC PROJECTILES AT SUPERSONIC SPEEDS	Final
	6. PERFORMING ORG. REPORT NUMBER

7. AUTHOR(s)	8. CONTRACT OR GRANT NUMBER(s)
Michael J. Nusca	

9. PERFORMING ORGANIZATION NAME AND ADDRESS	10. PROGRAM ELEMENT, PROJECT, TASK AREA & WORK UNIT NUMBERS
U.S. Army Ballistic Research Laboratory, ARDC ATTN: DRSMC-BLL (A) Aberdeen Proving Ground, Maryland 21005	RDT&E 1L162618AH80

11. CONTROLLING OFFICE NAME AND ADDRESS	12. REPORT DATE
US Army AMCCOM, ARDC Ballistic Research Laboratory, ATTN: DRSMC-BLA-S(A) Aberdeen Proving Ground, Maryland 21005	December 1983
	13. NUMBER OF PAGES
	56

14. MONITORING AGENCY NAME & ADDRESS(*if different from Controlling Office*)	15. SECURITY CLASS. *(of this report)*
	Unclassified
	15a. DECLASSIFICATION/DOWNGRADING SCHEDULE

16. DISTRIBUTION STATEMENT *(of this Report)*

Approved for public release; distribution unlimited.

17. DISTRIBUTION STATEMENT *(of the abstract entered in Block 20, if different from Report)*

18. SUPPLEMENTARY NOTES

19. KEY WORDS *(Continue on reverse side if necessary and identify by block number)*

Afterbody	Gyroscopic Stability
Flare	Dynamic Stability
Parabolized Navier-Stokes	Supersonic Flow
Projectile Aerodynamics	

20. ABSTRACT *(Continue on reverse side if necessary and identify by block number)*

A parametric study has been conducted for eight similar axisymmetric, spin stabilized projectile shapes. The aerodynamic and stability parameters of flared projectile afterbodies at freestream Mach numbers of 2, 3 and 4 and at an angle of attack of 2° have been determined. The projectiles under investigation had an ogive nose, a cylindrical midsection and one of three afterbodies: an extended cylinder, a boattail (conical frustum), and a boattail-flare (two conical frustums end to end). Total projectile lengths of 6 and 7 calibers have been

DD _{1 JAN 73} **1473** EDITION OF 1 NOV 65 IS OBSOLETE

20. ABSTRACT (Continued)

studied. Finite difference solutions of the Navier-Stokes equations, the method of characteristics, and semi-empirical models are used to predict normal force, static pitching moment, total drag, Magnus moment, roll damping and pitch damping. Estimations of gyroscopic and dynamic stability parameters are then made.
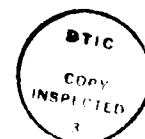
This study determined that the boattail-flare renders the ogive nose and cylindrical midsection projectile configuration more gyroscopically and dynamically stable than the conventional boattail afterbody. Results also showed that the boattail-flare afterbody decreases the Magnus moment but increases total drag therefore providing a stability advantage at the expense of reduced range. This stability advantage can be utilized in long spin-stabilized projectiles as well as long rod penetrators where fin stabilization has been replaced by a boattail-flare. Future work may be aimed at utilizing present computational techniques as a design tool in the use of a flared afterbody for stable, reduced range projectiles.

TABLE OF CONTENTS

LIST OF ILLUSTRATIONS

LIST OF ILLUSTRATIONS (continued)

I. INTRODUCTION

The long, slender, axisymmetric bodies that are conventionally used for spin-stabilized projectile designs consist of an ogive nose section followed by a constant diameter cylinder and a boattail. The ogive is similar in shape to a cone but typically has a smaller associated wave drag and has more volume for a payload. Secant ogives that are normally used are not tangent to the cylinder at the end of the nose section. In order to decrease base drag, a boattail is added. The boattail is a conical frustum that narrows the base to typically 75% of the cylindrical body diameter. This description characterizes the conventional spin-stabilized secant-ogive cylinder boattail (SOCBT) projectile. Afterbody designs that statically stabilize nonspinning projectiles are lifting surfaces of two types: thin fins and conical flares. Fins positioned as a tail generate normal force to statically stabilize the projectile, whereas conical flared afterbodies generate high pressure regions and move the center of pressure rearward, behind the center of gravity.

The purpose of this study is to evaluate the ability of a boattail-flare (see Figure 1) to improve the stability of the SOCBT configuration. Computational methods are used to solve the parabolized Navier-Stokes equations in the flowfield around the projectile. Predictions of static pitching moment, drag force, and roll damping, Magnus and pitch damping moments are made to define the effects of the boattail-flare afterbody on the aerodynamics of the ogive-cylinder projectile.

II. BACKGROUND

The gyroscopic stability of a spin-stabilized projectile can be assessed by computing s_g, the gyroscopic stability factor.[1]

$$s_g = \frac{2 \; (pd/V)^2 \; I_x^2}{\pi \rho \; I_y \; d^5 \; C_{M\alpha}} \tag{1}$$

where;

I_x = axial moment of inertia, kg - m³

I_y = transverse moment of inertia, kg - m³

pd/V = dimensionless axial spinrate

p = axial angular velocity, rad/sec

ρ = air density, kg - m³

d = maximum body diameter, m

---

1. Murphy, C.H., "Free Flight Motion of Symmetric Missile," U.S. Army Ballistic Research Laboratory Report No. 1216, Aberdeen Proving Ground, Maryland 21005, July 1963 (AD 442757).

$$V \quad = \quad \text{airspeed, m/sec}$$

$$C_{M\alpha} \quad = \quad \text{static moment coefficient, per radian}$$

If $0 < s_g < 1$ the projectile is gyroscopically unstable. Note that s_g is inversely proportional to air density; therefore, projectiles that are gyroscopically stable for standard atmospheric conditions may not be stable under nonstandard temperature and pressure. Due to this as well as other uncertainties in computing s_g, many designers have set 1.3 as a lower limit on gyroscopic stability.[2]

An additional requirement for spin-stabilized projectiles is that they be dynamically stable. The dynamic stability of a projectile is defined by Murphy[1] as

$$s_d = \frac{2(C_{N\alpha} - C_D) + 2\, k_x^{-2}\, C_{MP\alpha}}{C_{N\alpha} - 2\, C_D - k_y^{-2}\, (C_{Mq} + C_{M\dot{\alpha}})} \tag{2}$$

where; $C_{N\alpha}$ = normal force coefficient slope per radian

C_D = total drag force coefficient

$C_{MP\alpha}$ = Magnus moment coefficient slope per radian

$C_{Mq} + C_{M\dot{\alpha}}$ = pitch damping coefficient

k_x = axial radius of gyration

k_y = transverse radius of gyration

The range of values of s_d for dynamic stability are also given by Murphy[1] and are found to be a function of the reciprocal of the gyroscopic stability.

$$1/s_g = s_d\,(2 - s_d) \tag{3}$$

---

2. "Engineering Design Handbook - Design for Control of Projectile Flight Characteristics," Headquarters, US Army Materiel Command, September 1966.

III. COMPUTATIONAL TECHNIQUE

Evaluation of the stability of secant ogive-cylinder projectiles with a boattail, or boattail-flare afterbody, requires the calculation of the aerodynamic forces (normal, drag, and Magnus) and moments (pitching, Magnus, and roll damping). These parameters were determined using three techniques: solution of the parabolized Navier-Stokes equations, the method of characteristics, and semi-empirical models.

Recent papers[3,4,5,6,7] describe the application of the thin-layer parabolized Navier-Stokes (PNS) computational technique to predict the flow about slender bodies of revolution with sharp noses at supersonic velocities. The PNS technique was used in this study to yield the aerodynamic coefficients necessary for the evaluation of static, gyroscopic and dynamic stability.

Schiff and Sturek[4] have employed the PNS computational technique to solve for the flowfield about a sharp body of revolution and have made comparisons with experimental data. Computed and measured pressure data in both the axial and circumferential directions were consistent.

The PNS solutions do not compute the base flow region. Therefore, calculation of the base drag was performed using the method described by Roache and Mueller.[8] The base flow computation was started upstream of the afterbody

3. Schiff, L.B., and Steger, J.L., "Numerical Simulation of Steady Supersonic Viscous Flow," AIAA Journal, Vol. 18, No. 12, December 1980, pp. 1421-1430.

4. Schiff, L.B., and Sturek, W.B., "Numerical Simulation of Steady Supersonic Flow over an Ogive-Cylinder-Boattail Body," ARBRL-TR-02363, US Army Ballistic Research Laboratory, Aberdeen Proving Ground, Maryland 21005, September 1981 (AD A106060).

5. Sturek, W.B., and Schiff, L.B., "Computations of the Magnus Effect for Slender Bodies in Supersonic Flow," ARBRL-TR-02384, US Army Ballistic Research Laboratory, Aberdeen Proving Ground, Maryland 21005, December 1981 (AD A110016).

6. Sturek, W.B., and Mylin, D.C., "Computational Study of the Magnus Effect on Boattailed Shell," AIAA Journal, Vol. 20, No. 10, October 1982, pp. 1462-1464.

7. Sturek, W.B., Guidos, B., and Nietubicz, C.J., "Navier-Stokes Computational Study of the Influence of Shell Geometry on the Magnus Effect at Supersonic Speeds," ARBRL-TR-02501, US Army Ballistic Research Laboratory, Aberdeen Proving Ground, Maryland 21005, June 1983 (AD A130630).

8. Mueller, T.J., and Kayser, L.D., "A Method of Determining the Turbulent Base Pressure in Uniform and Non-Uniform Supersonic Flows," ARBRL-TR-02374, US Army Ballistic Research Laboratory, Aberdeen Proving Ground, Maryland 21005, October 1981 (AD A107318).

using local velocity profiles from the PNS computation and yielded the ratio of base to freestream pressure from a method of characteristics solution. For the cylindrical and boattailed afterbodies, the solution was started at the end of the cylindrical portion of the projectile, whereas the solution for the boattail-flare afterbody was started at the end of the flare with the characteristic lines extending into the base region.

A second auxiliary calculation was required for the pitch damping coefficients used in determining the dynamic stability factor, s_d. (See Equation 2.)

A semi-empirical technique developed by Devan and Mason[9] computes the pitch damping coefficient based on trends in wind tunnel and flight test data for this class of axisymmetric bodies.

IV. PROCEDURE

To adequately evaluate the effectiveness of different projectile design a parametric study was undertaken using the eight different shapes shown Figure 1 and described in Table 1. Figure 2 is a schematic of the projecti shapes studied grouped according to geometric similarity. All data generat in the investigation are also grouped in this fashion. The projectile shap had the same nose section (ogive) and differed only in the length of t cylinder and afterbody sections. Included in study were both the convention boattail and unconventional boattail-flare afterbody.

TABLE 1. PROJECTILE PHYSICAL PROPERTIES. MATERIAL DENSITY ASSUMED 2.77×10^{-6} kg/mm^3 (ALUMINUM)

	L1	(mm) L2	L3	(Kg) Mass	(Kg - mm^2) Ix	Iy
SOC1/2	171.6	0	0	1.74	6.38×10^2	1.08×10^4
SOC3	228.8	0	0	2.14	8.04×10^2	2.23×10^4
SOCBT1	114.4	57.2	0	1.65	5.75×10^2	9.51×10^3
SOCBT2	57.2	114.4	0	1.40	4.38×10^2	7.28×10^3
SOCBT3	114.4	114.4	0	1.81	6.03×10^2	1.39×10^4

9. Devan, L., and Mason, L.A., "Aerodynamics of Tactical Weapons to Mach Number 8 and Angle of Attack 180°: Part II, Computer Program and Users Guide," N.S.W.C. TR 81-358, September 1981.

TABLE 1. (continued)

SOCBTF1	114.4	28.6	28.6	1.69	6.02×10^2	1.02×10^4
SOCBTF2	57.2	57.2	57.2	1.56	5.11×10^2	9.48×10^3
SOCBTF3	114.4	57.2	57.2	1.96	6.77×10^2	1.86×10^4

Because of these geometric similarities the PNS code was advanced over the 3 caliber ogive and onto the cylindrical section for 1 caliber. The resulting data were used to restart the computation over different afterbodies. In this way the computational time was reduced from the time that would be required if the PNS solution was started from the nose of each of the eight bodies. The computations were carried out for an angle of attack of 2° and a nondimensional spinrate of 0.19 (used for Magnus computations).

Using the Roache-Mueller method, the plane of data supplied by the PNS solution at the end of the body was advanced into the base region to calculate base pressure. Base pressure data, in the form of a ratio of base to freestream pressure, was converted to base drag coefficient form[10] using:

$$C_{DB} = \frac{2\ d^2\ (1 - P_B/P_\infty)}{\gamma M_\infty^2} \qquad (4)$$

where d = base diameter in calibers
           M_∞ = freestream Mach number

The semi-empirical method of Devan and Mason was used to compute pitch damping for the ogive-cylinder (SOC1, 2, 3) and ogive-cylinder-boattail (SOCBT1, 2, 3) bodies, the data base did not allow accurate computations of the boattail-flare bodies (SOCBTF1, 2, 3). The pitching moment of a boattail-flare afterbody was assumed to be the same as that of the boattailed body of equal length (e.g., SOCBTF1 and SOCBT1). Flares in general have been shown to

---

10. McCoy, R.L., "McDrag - A Computer Program for Estimating the Drag Coefficients of Projectiles," ARBRL-TR-02293, US Army Ballistic Research Laboratory, Aberdeen Proving Ground, Maryland 21005, February 1981 (AD A098110).

increase a projectile's pitch damping;[11] predictions of this coefficient are therefore conservative.

The computed data were reduced to the following aerodynamic coefficients. Total drag was obtained from the summation of viscous, pressure, and base drag coefficients. Normal force slope, $C_{N\alpha}$ (assumed to be linear), was obtained by dividing the normal force coefficient by .0349 radian ($2°$). Pitching moment slope, $C_{M\alpha}$, and Magnus moment slope, $C_{MP\alpha}$, were obtained by referencing the moment coefficient to a point 3.6 calibers from the projectile nose in all cases, and dividing by .0349 radian. Roll damping coefficient, C_{ℓ_p} was obtained directly from the PNS computation. Variations of dimensionless spin-rate, pd/V, were evaluated from Equation 1 assuming s_g = 1.3, while dynamic stability was evaluated from Equation 2.

V. RESULTS AND DISCUSSION

The aerodynamic stability of the projectile configurations was studied in three ways: static, gyroscopic, and dynamic stability. Static stability is defined in terms of the static pitching moment, gyroscopic stability in terms of s_g and dimensionless spinrate, and dynamic stability as defined in Equation 2.

Typical wall pressure distributions at Mach 3 (angle of attack $2°$) are shown in Figure 3 for one group of configurations, SOC2, SOCBT2, SOCBTF2. The effect of the boattail-flare afterbody is immediately apparent from the dramatic pressure recovery that occurs over the flared portion (Figure 3c). The higher pressure on the windward side of the projectile is due to the angle of attack and is responsible for the projectile's normal force. Higher leeward pressure on the boattail detracts from the total normal force of the projectile (Figure 3b). A large pressure recovery for the boattail-flare is shown in Figure 3c.

The axial distribution of normal force for this group of configurations is shown in Figure 4. The local normal force rises over the 3-caliber ogive and 1-caliber cylinder, decreases sharply over the 2-caliber boattail but is partially recovered when one caliber of the boattail is flared.

The wall pressure and normal force recovery effect of the boattail-flare afterbody depends largely on the value of freestream Mach number. Using the SOCBTF1 configuration as an example, Figures 5a-c show the dramatic change in wall pressure recovery over the .5-caliber flare. At Mach 2 (Figure 5a) wall pressure recovery is minimal and the pressure difference from windward to leeward side is negligible. For Mach 3 and 4 (Figures 5b and 5c) the effect of the flare is significant, producing a large difference between windward and

11. Robinson, M.L., "Boundary Layer Effects in Supersonic Flow Over Cylinder-Flare Bodies," Australian Defense Scientific Service Weapons Research Establishment Report No. 1238, July 1974.

leeward wall pressures. When these pressure differences are converted to nor-
mal force distributions, the effect of Mach number is again observed (Figures
6a-c).

A. Static and Gyroscopic Stability

The ability of the boattail-flare afterbody to augment the normal force
of the secant ogive cylinder projectile radically changes the static pitching
moment. Integration of the normal force distribution yields a total normal
force located at the center of pressure. The static pitching moment is
defined by this force and the difference between the center of pressure and
center of gravity locations. Comparisons can be made between the SOC, SOCBT
and SOCBTF configurations on the basis of static pitching moment because this
moment is referenced to the same point for each body (3.6 calibers from the
nose as described in the Section IV). Figure 7a, b, and c compare the pitch-
ing moment characteristics of the cylinder, boattial and boattail-flare after-
bodies in the three groups of configurations.(Recall Figure 2.) Consistent
with the axial distribution of normal force, the SOC and SOCBTF configurations
in each group exhibit the lowest pitching moment coefficient (significantly
lower than the SOCBT). Comparing all flared bodies, SOCBTF, Figure 7d shows
that the SOCBTF1 has the smallest pitching moment coefficient for all but Mach
4.

Of the three flared configurations the SOCBTF1 has the shortest boattail-
flare afterbody length; the pitching moment performance of this configuration
relative to configurations with longer flares (e.g., SOCBTF3) must therefore
be explained. Wall pressure distributions reveal that the shorter flare main-
tains a large difference between windward and leeward pressure over its entire
length whereas the longer flares allow the flow to expand over their length
thus losing normal force.(Compare Figure 3c between 5 and 6 calibers and
Figure 5b between 5.5 and 6 calibers.) The SOCBTF1 configuration is unique in
that it has the shortest boattail and therefore does not generate the loss in
normal force characteristic of long boattails.(Review Figures 3b and 5.) As
the freestream Mach number increases to Mach 4, the long flare of the SOCBTF3
generates increasingly more normal force and finally overcomes the loss asso-
ciated with its long boattail. However, the SOCBTF3 is the greatest normal
force and the smallest moment arm (cg-cp) and is therefore subjected to the
smallest pitching moment at Mach 4.

From computed pitching moment data and an assumed s_g of 1.3, dimension-
less spinrates (pd/V) can be determined from Equation 1 as described in Sec-
tion IV. Figure 8a, b and c show that pd/V decreases with freestream Mach
number for all configurations with the lowest pd/V associated with the SOC and
SOCBTF. In each case the boattail-flare afterbody reduced pd/V below that
required of the boattail afterbody but not as low as the configuration without
an afterbody (SOC). The shortest boattail-flare afterbody (SOCBTF1), however,
shows a pd/V comparable to the corresponding SOC configuration (Figure 8c).
In addition the SOCBTF1 shows the lowest required pd/V of all flared after-
bodies (Figure 8d).

B. Dynamic Stability

Dynamic stability as defined in Equation 2 requires the aerodynamic coefficients of drag, normal force, Magnus moment, and pitch damping. Evaluation of these coefficients will precede discussion of the dynamic stability factor, S_d.

Figures 9a-d compare the drag coefficients of all configurations. As mentioned in the proceedure section, drag coefficient is the algebraic sum of viscous drag and pressure drag (from PNS computation) along with base drag (from Roache-Mueller). The boattail afterbody configurations (SOCBT) have the least drag due to the narrowing of the base. This narrowing causes a flow expansion that decreases the base pressure (P_B/P_∞ decreases) but also geometrically decreases the base diameter (d_B). The combined effect decreases base drag. (See Equation 4.)

The boattail-flare afterbody exhibits a significantly larger drag coefficient in all cases but for the SOCBTF1. The source of this drag penalty is two-fold: the pressure drag associated with the oblique shock formed at the boattail-flare junction and the higher base drag associated with the larger diameter base. Of all flared configurations, however, the SOCBTF1 shows the smallest drag rise (Figure 9d).

Figures 10a-b compare the Magnus moment coefficient slope of all configurations. Consider a spinning axisymmetric body at angle of attack. The component of freestream velocity perpendicular to the body (cross flow) is decelerated on the side that opposes spin and is accelerated on the side that is coincident with spin. This difference in velocity across the body gives rise to a difference in pressure and a side force develops, the Magnus force. This force becomes more significant as the boundary layer thickens on the aft end of the projectile. This is especially true of boattail afterbodies where the expanded flow accelerates the boundary layer growth. In contrast a flare generates an adverse pressure gradient and thins the boundary layer.[11] In this study it was expected that the SOCBT configuration would have the highest Magnus moment with the SOCBTF configuration having the lowest. This is supported in Figure 10. Comparing all of the SOCBTF configurations the shortest flare, SOCBTF1, had the smallest Magnus moment (Figure 10d).

The roll damping coefficient data are illustrated in Figures 11a-b. Due to the viscous boundary layer a shearing force is generated on the projectile surface in the direction opposite the spinrate. (Hence, the coefficient is usually negative.) Because the roll damping coefficient arises from viscous shear, it is directly proportional to the velocity component tangent to the body surface. Using an aeroballistic coordinate system, the component of velocity in the x-direction (along the body axis, positive rearward) is designated u, the component perpendicular to the body axis is v, and the third component to form a right-handed axis system is w. Roll damping coefficient is then proportional to dw/dy. As the radius of the spinning body decreases, surface velocity decreases also ($w = \Omega r$). As Figure 11 illustrates the SOC design has the largest roll damping because it has the greatest body diameter from nose to base. When a boattail afterbody is used (SOCBT) the roll damping decreases slightly as the body radius decreases. The boattail-flare afterbody design increases roll damping to a small degree because it has an increased

14

body slope -- but the SOCBTF has less roll damping than the SOC with a constant diameter shape.

From the discussion above it is also clear that roll damping is proportional to surface area -- the larger a body is the more viscous shear is generated. Figure 11a, that represents the longest group of projectiles (the SOC3, SOCBT3, SOCBTF3 are 7 calibers long), also shows the largest roll damping. Figures 11b, and c represent the two groups of projectiles that are 6 calibers in length and therefore show less roll damping. The increase in roll damping predicted for the boattail-flare afterbody could be viewed as a disadvantage to the design if it were not for the small magnitude of that increase. Figure 11d illustrates that the boattail-flare afterbody design that leads to the smallest increase in roll damping is not the shortest flare (which has been the pattern up to this point) but the one with the shortest cylindrical section, SOCBTF2. Reviewing Figure 2, it would seem that the SOCBTF2 has the smallest overall amount of surface area.

With the aerodynamic coefficients of drag and Magnus moment, the dynamic stability factor, s_d, as given in Equation 2, can be evaluated. Table 2 lists the values of s_d grouped by geometric similarity. Dynamic stability was increased for all boattail-flare projectiles when compared to the straight cylinder bodies. The boattail-flare afterbody increased s_d in only a few cases when compared to the boattail bodies. At Mach 4, the boattail-flare consistently led to a more dynamically stable projectile. For the first group, the SOCBTF1 increased the stability of the projectiles for all of Mach numbers.

TABLE 2. DYNAMIC STABILITY FACTORS (s_d)*

	MACH = 2	MACH = 3	MACH = 4
SOC1	.273	.292	.293
SOCBT1	.353	.365	.360
SOCBTF1	.360	.376	.378
SOC2	.273	.292	.293
SOCBT2	.349	.367	.365
SOCBTF2	.341	.362	.384
SOC3	.307	.321	.339
SOCBT3	.427	.419	.428
SOCBTF3	.414	.398	.430

*BOXES INDICATE THOSE CONFIGURATIONS AND MACH NUMBERS AT WHICH THE BOATTAIL-FLARE AFTERBODY HAS INCREASED DYNAMIC STABILITY.

15

The dynamic stability factor involves many aerodynamic coefficients, but is defined in a complicated manner. Platou[12] has attempted to determine the relative importance of the individual aerodynamic coefficients used with dynamic stability. Examining s_d in a parametric manner, Platou concluded:

(1) $C_{N\alpha}$ and C_D have only a small influence on s_d except when $C_{N\alpha} - 2C_D$ is maximum (i.e., $C_{N\alpha}$ is maximum and C_D is minimum) s_d is maximum.

(2) s_d is maximum when the transverse moment of inertia, Iy, is minimum.

(3) s_d is maximum when Magnus moment slope, $C_{MP\alpha}$, is minimum.

(4) If pitch damping, $C_{Mq} + C_{M\dot{\alpha}}$, is minimum then s_d is maximum. Also, if pitch damping is maximum then the relative influence of $C_{MP\alpha}$ on s_d is increased.

The data computed by this study showed the following trends for the flare shapes:

	Iy	$C_{N\alpha}$	C_D	$C_{MP\alpha}$	$C_{Mq} + C_{M\dot{\alpha}}$
smallest	SOCBTF2	SOCBTF2	SOCBTF1	SOCBTF1	SOCBTF1
↕	SOCBTF1	SOCBTF3	SOCBTF2	SOCBTF2	SOCBTF2
largest	SOCBTF3	SOCBTF1	SOCBTF3	SOCBTF3	SOCBTF3

Platou's conclusions can be used to explain the findings illustrated in Table 2. As mentioned, all projectiles showed an increase in the dynamic stability at Mach 4. Examining the data generated in this study, it has been shown that:

(1) Magnus moment slope was minimum at Mach 4 for all projectile designs studied.

(2) Pitch damping was essentially independent of Mach number.

(3) At Mach 4 the term $C_{N\alpha} - 2C_D$ is a maximum.

Also discussed was the increase in dynamic stability generated by the SOCBTF1 for the first group of configurations at all Mach numbers. Examining the flare data generated in this study it was shown that:

---

12. Platou, A.S., "The Influence of the Magnus Moment on the Dynamic Stability of a Projectile," ARBRL-MR-2155, US Army Ballistic Research Laboratory, Aberdeen Proving Ground, Maryland 21005, January 1972 (AD 738016).

(1) For all Mach numbers the SOCBTF1 has the highest $C_{N\alpha}$ and the lowest C_D, and therefore has the greatest value for the term $C_{N\alpha} - 2C_D$.

(2) For all Mach numbers the SOCBTF1 has the smallest Magnus moment slope.

(3) For all Mach numbers the SOCBTF1 has the smallest pitch damping.

VI. CONCLUSION

An investigation of the aerodynamics and stability of a flared afterbody for axisymmetric projectiles at supersonic speeds has been completed using computational fluid dynamic methods to predict the aerodynamic coefficients of interest. The parametric nature of the study has lead to the evaluation of the characteristics of the boattail-flare relative to the conventional SOCBT design. Although all of the three SOCBTF designs studied can be characterized by similar conclusions, the SOCBTF1 (having the shortest boattail and flare) has been shown to yield:

(1) The smallest static pitching moment coefficient and required spin-rate, therefore the greatest degree of static stability, of all designs with afterbodies (excluding the SOC designs).

(2) The greatest degree of dynamic stability enhancement of all design groups studied (independent of Mach number).

(3) The least Magnus moment of all designs studied and the smallest rise in total drag and roll damping of all designs studied with boattail-flare afterbodies.

With the reduction in the static instability of the spin-stabilized projectile provided by the boattail-flare afterbody, the projectile designer is afforded a greater degree of freedom in choosing values of spinrate, (or gyroscopic stability factor), axial and transverse moments of inertia. Even though the boattail-flare afterbody will allow the designer to reduce spinrate and still achieve gyroscopic stability (or hold spinrate constant and gain more gyroscopic stability) these degrees of freedom are not usually available. Rather, the projectile designer is given a minimum value of s_g and axial spin-rate suitable for the atmospheric operating conditions and the type of gun tube that will be used for firing, and asked to meet these parameters with a projectile that will also carry a given payload. The designer can then use the boattail-flare afterbody to extend the range of values over which the axial and transverse moments of inertia may vary. (Axial moment can be decreased and the transverse moment can be increased.)

Although the present investigation has established the aerodynamic and stability characteristics of a subcaliber flare (boattail-flare) afterbody for spin-stabilized projectiles, subsequent work may demonstrate further application to other ballistic projectile designs.

It has already been shown that the length (transverse moment of inertia) of spin-stabilized projectiles with the boattail-flare afterbody can be

increased without the loss of gyroscopic stability. Current research is applying the subcaliber flare to long spin-stabilized projectiles with a high density penetrator core as well as long rod penetrator fin-stabilized projectiles where a long boattail followed by a subcaliber flare replaces the fins.

With the present computational technique applied to a flare, future work could investigate the application of a flared afterbody to long projectiles that require stable flights without spin, in addition to enhanced drag for short range.

18
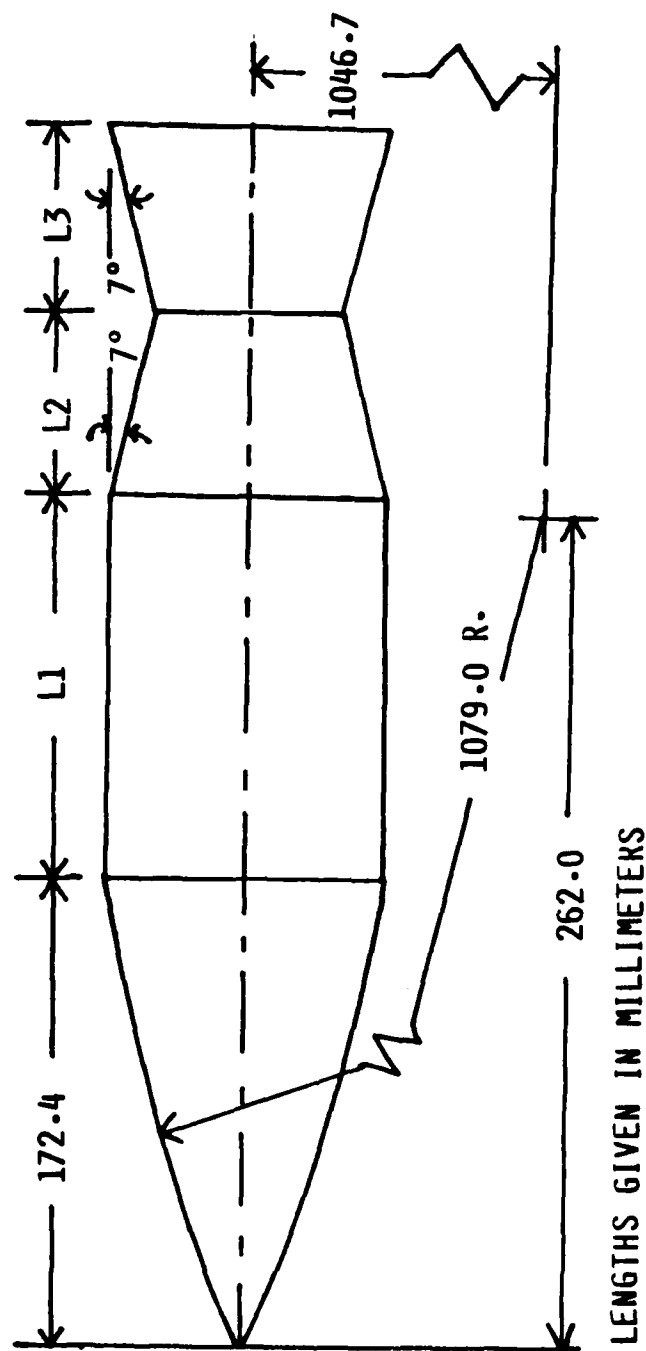
Figure 1. Projectile Geometry

LENGTHS GIVEN IN MILLIMETERS
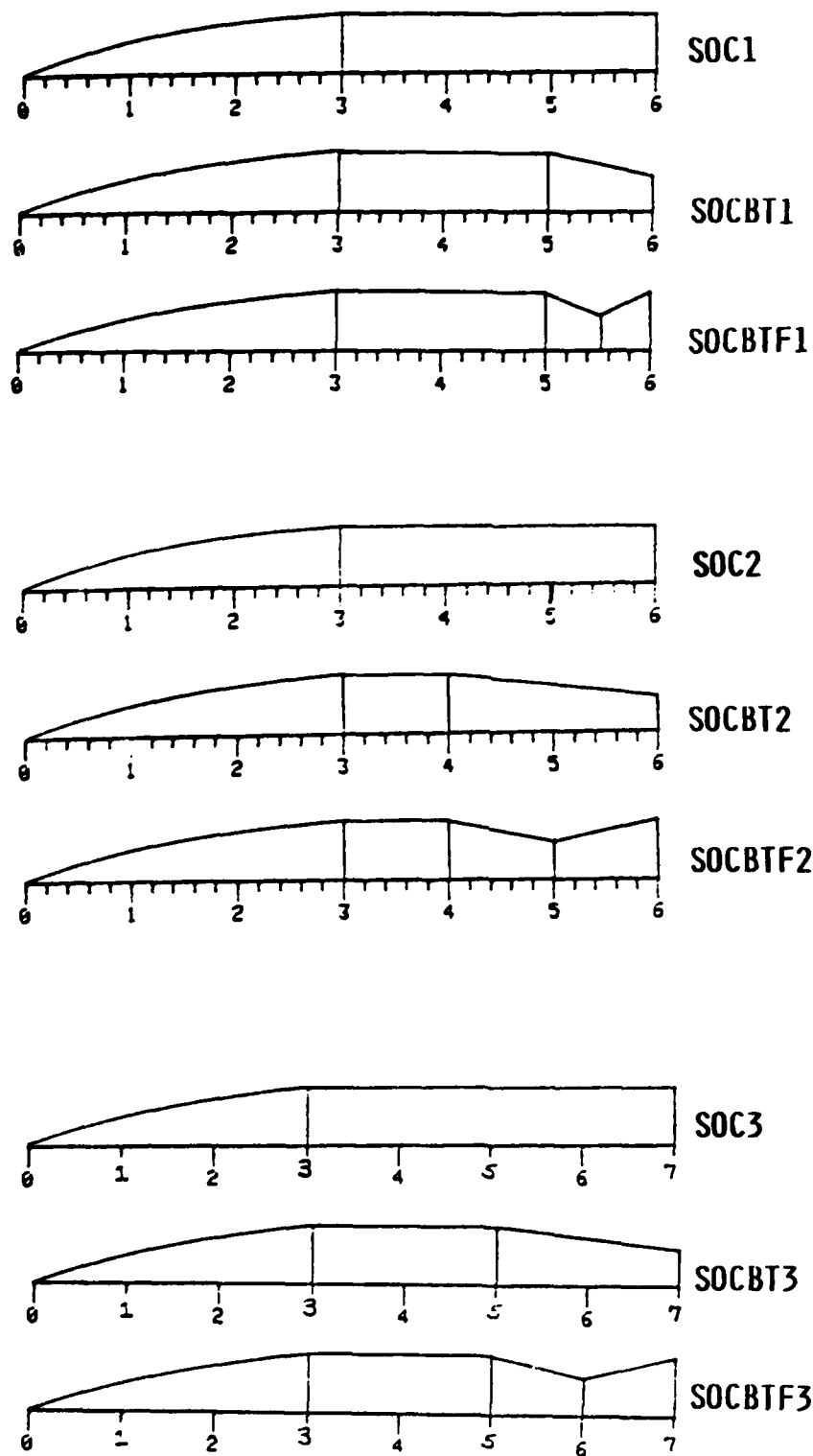
Figure 2.   Schematic Drawings of Projectile Groups
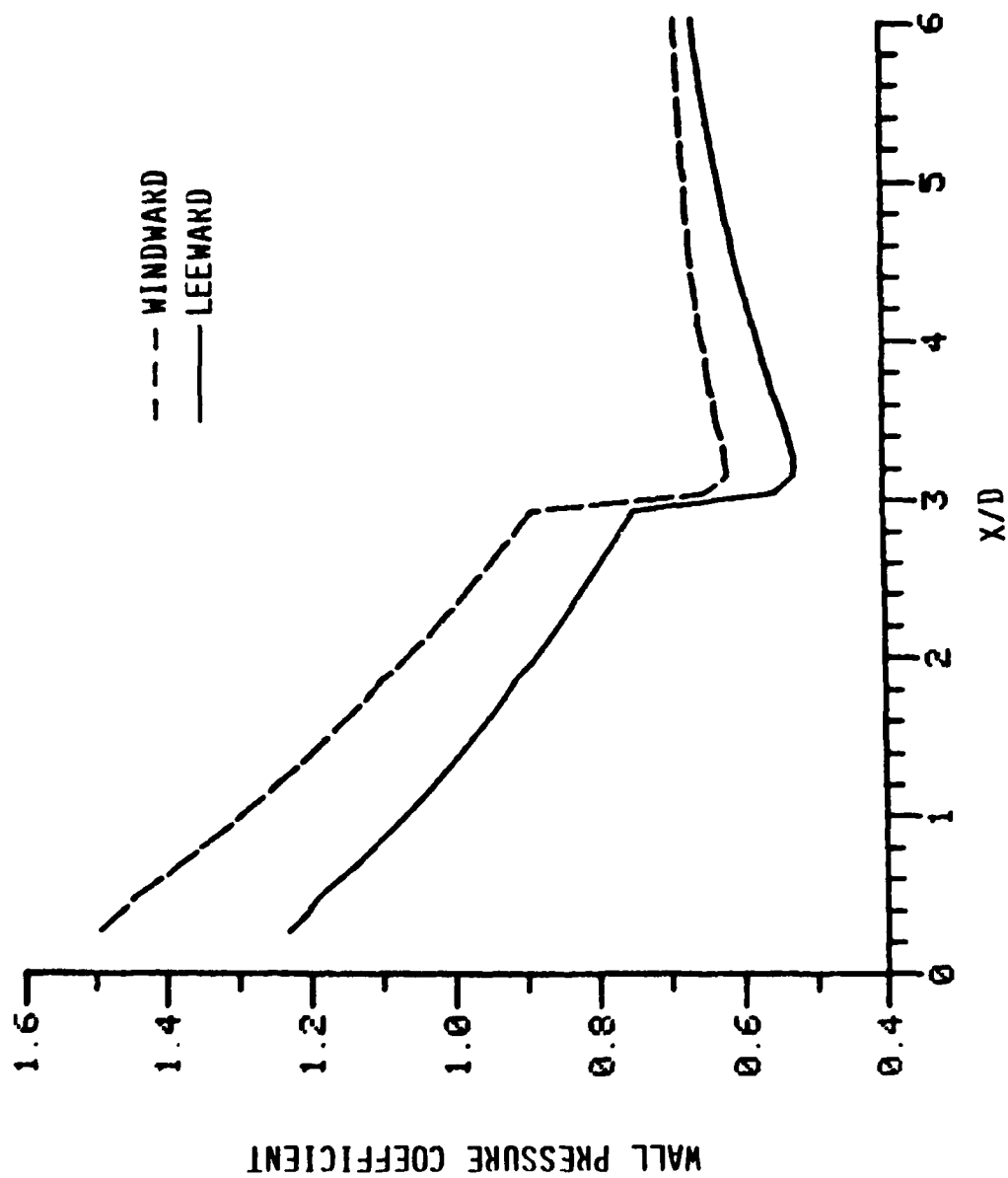
Figure 3. Axial Surface Pressure Distributions; M = 3.0, α = 2°

a. SOC2
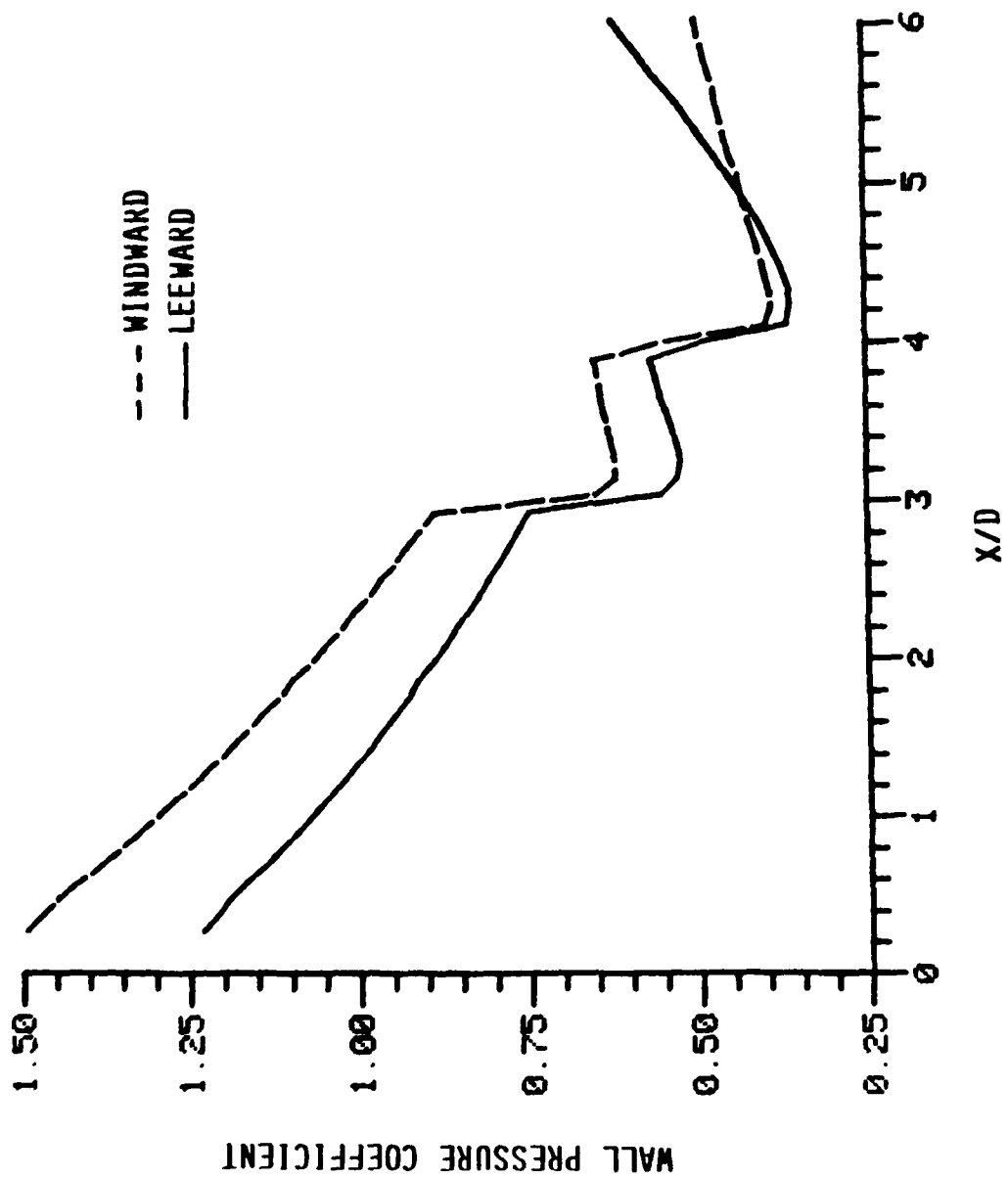
Figure 3. Continued

b. SOCBT2
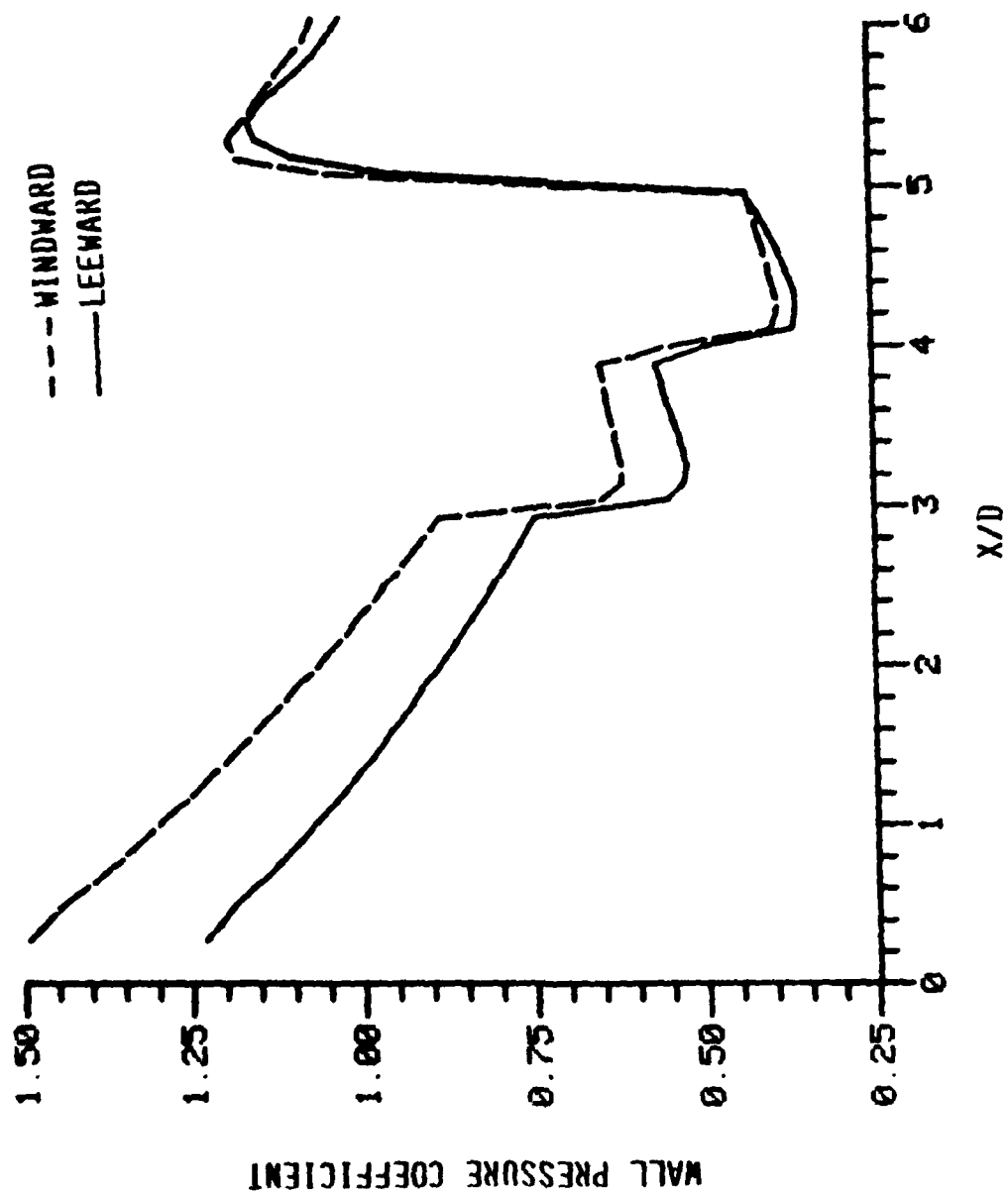
Figure 3. Continued

c. SOCBTF2

23
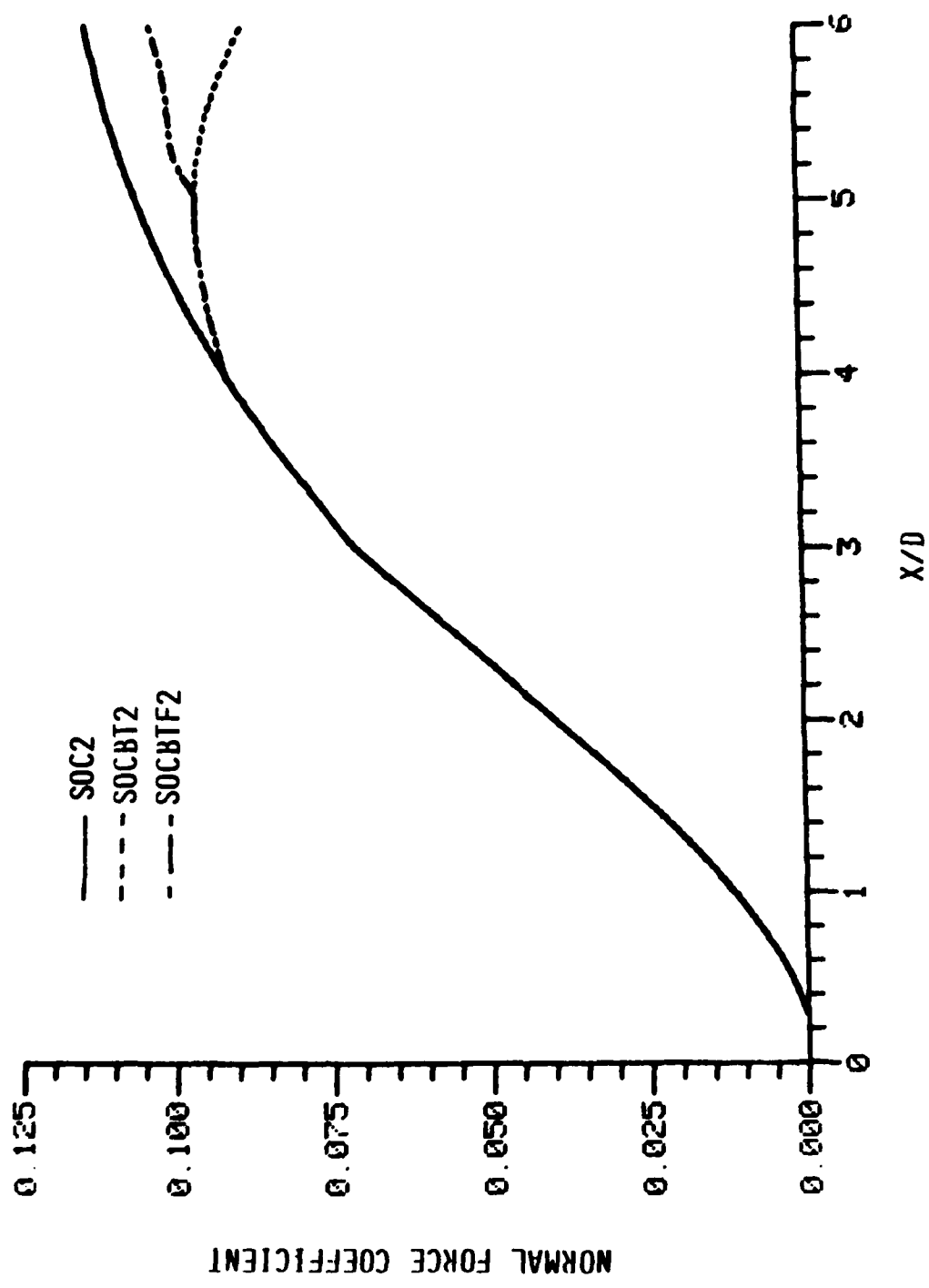
Figure 4. Axial Normal Force Distributions; M = 3.0, α = 2°, SOC2, SOCBT2, SOCBTF2

24
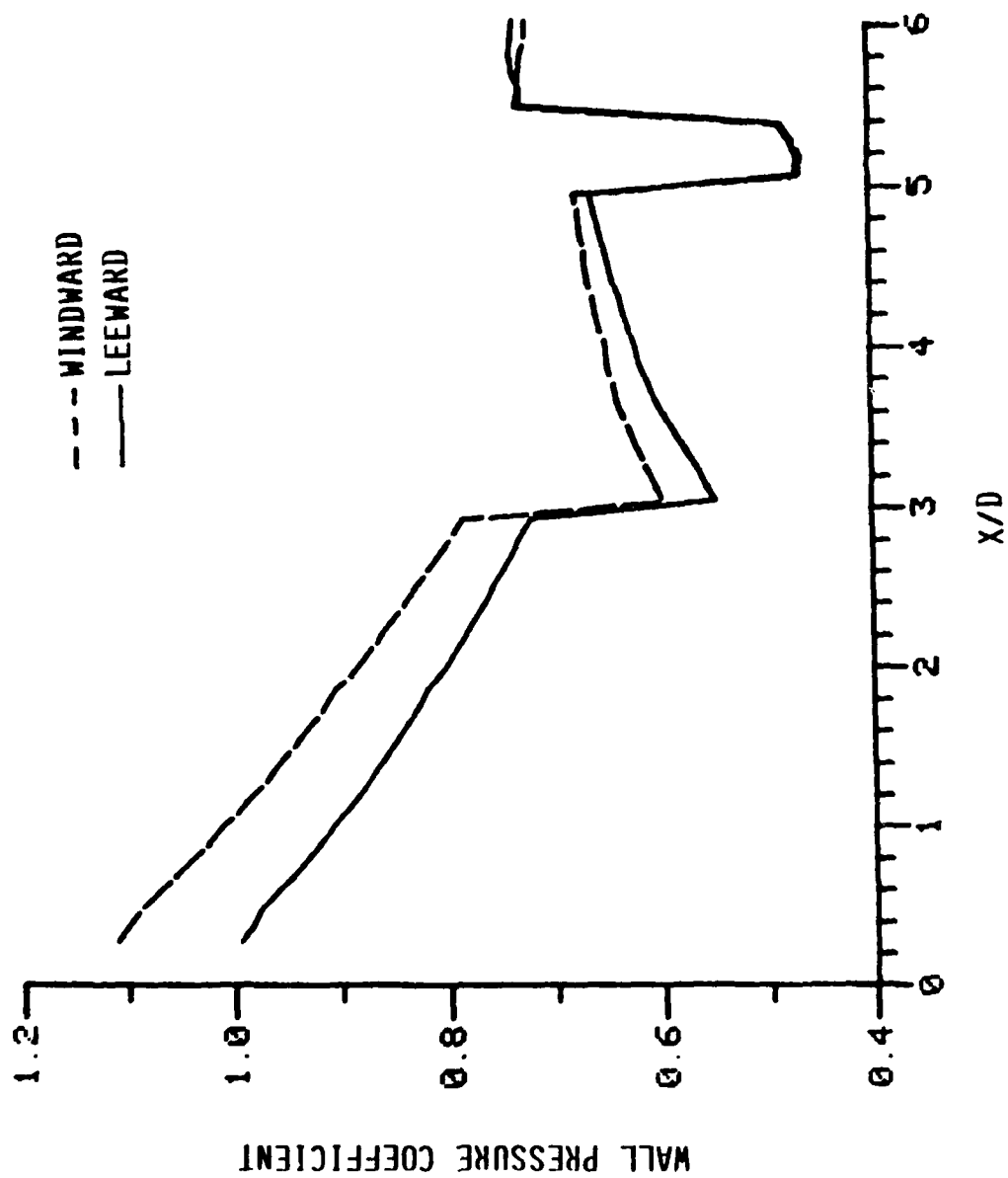
Figure 5. Axial Surface Pressure Distributions; SOCBTF1, α = 2°
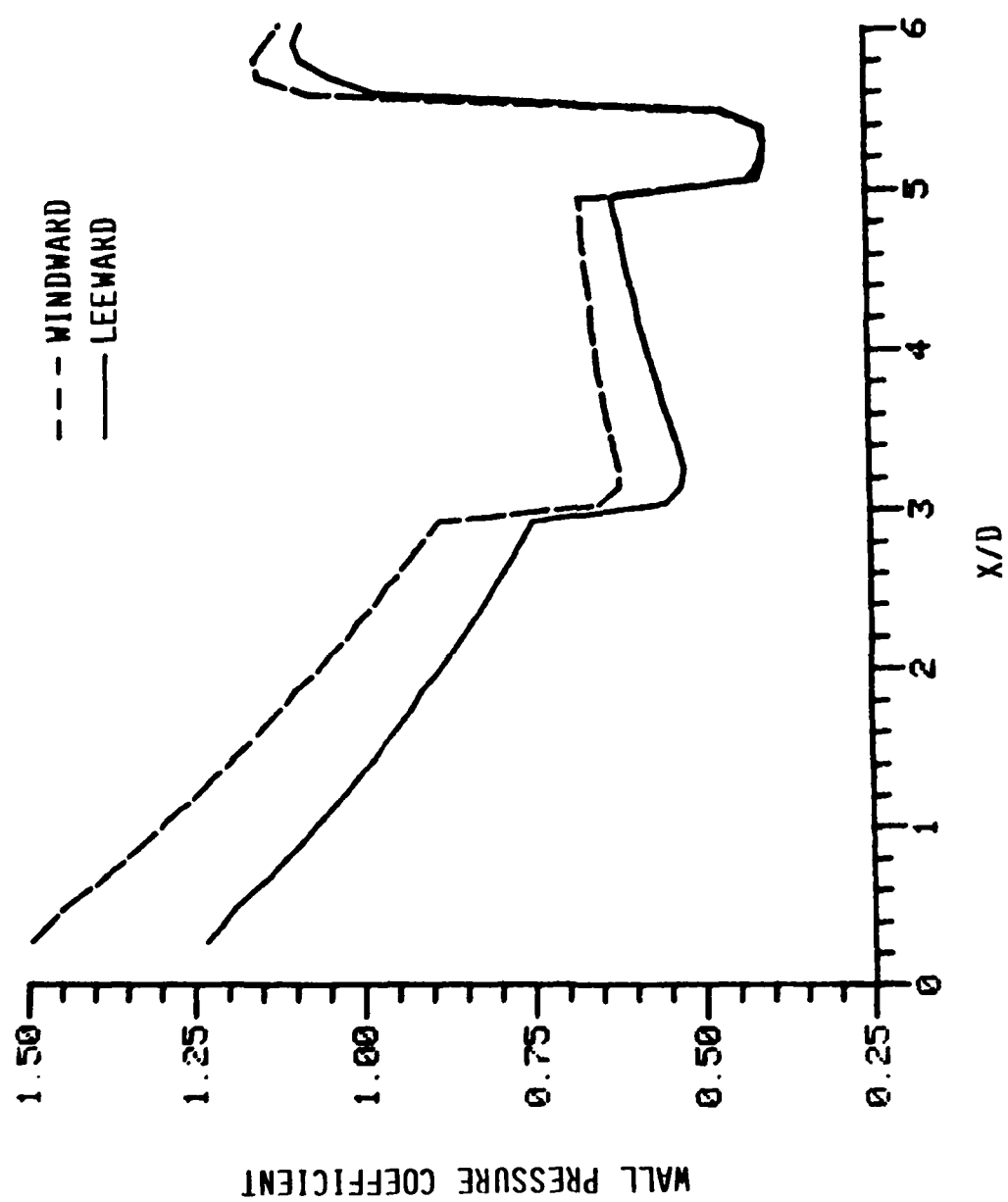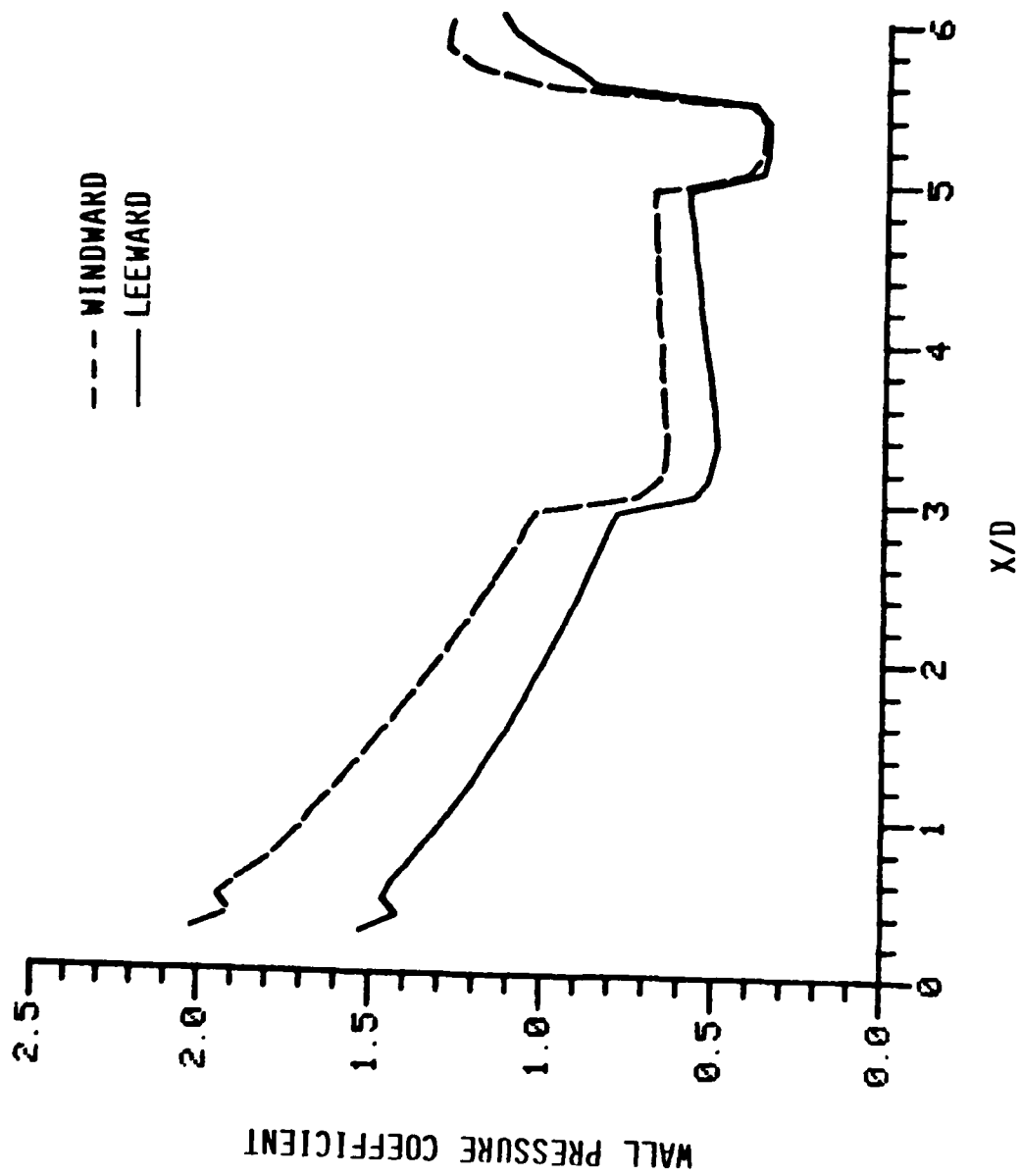
a. Mach = 2

Figure 5. Continued

b. Mach = 3

26

Figure 5. Continued

c. Mach = 4

27
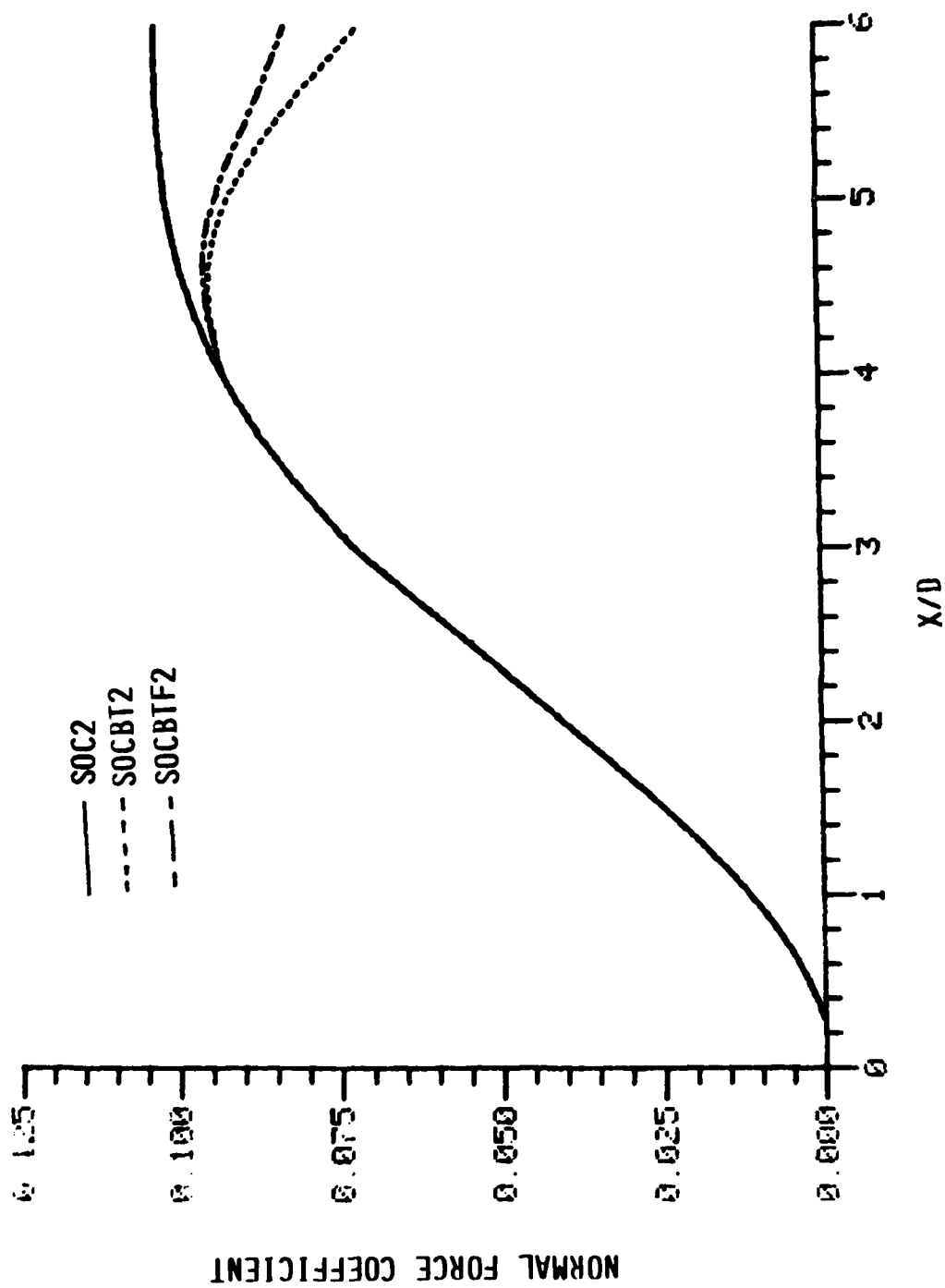
Figure 6.   Axial Normal Force Distributions; SOC2, SOCBT2, SOCBTF2, α = 2°

a.   Mach = 2

28
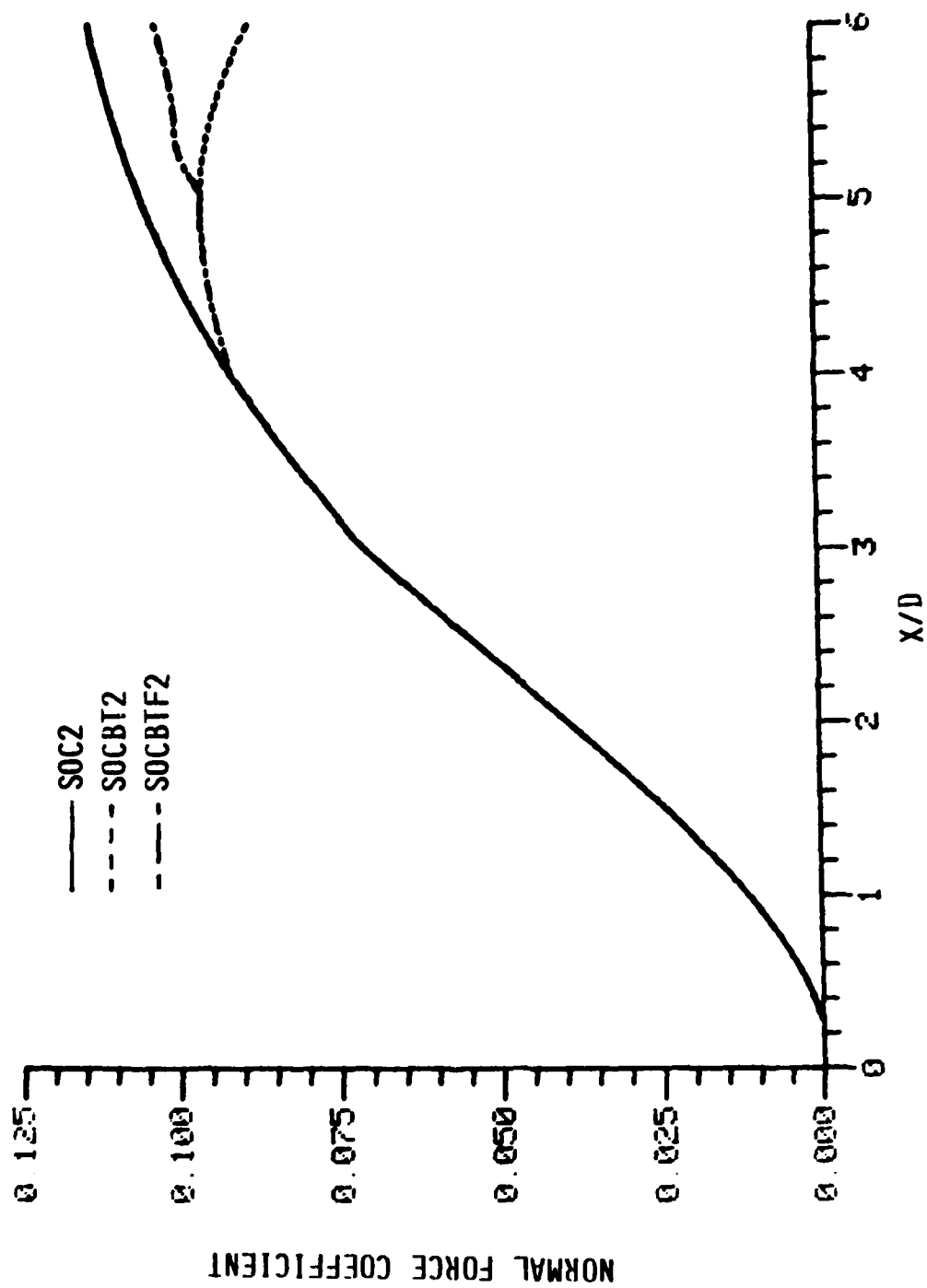
Figure 6. Continued

b. Mach = 3
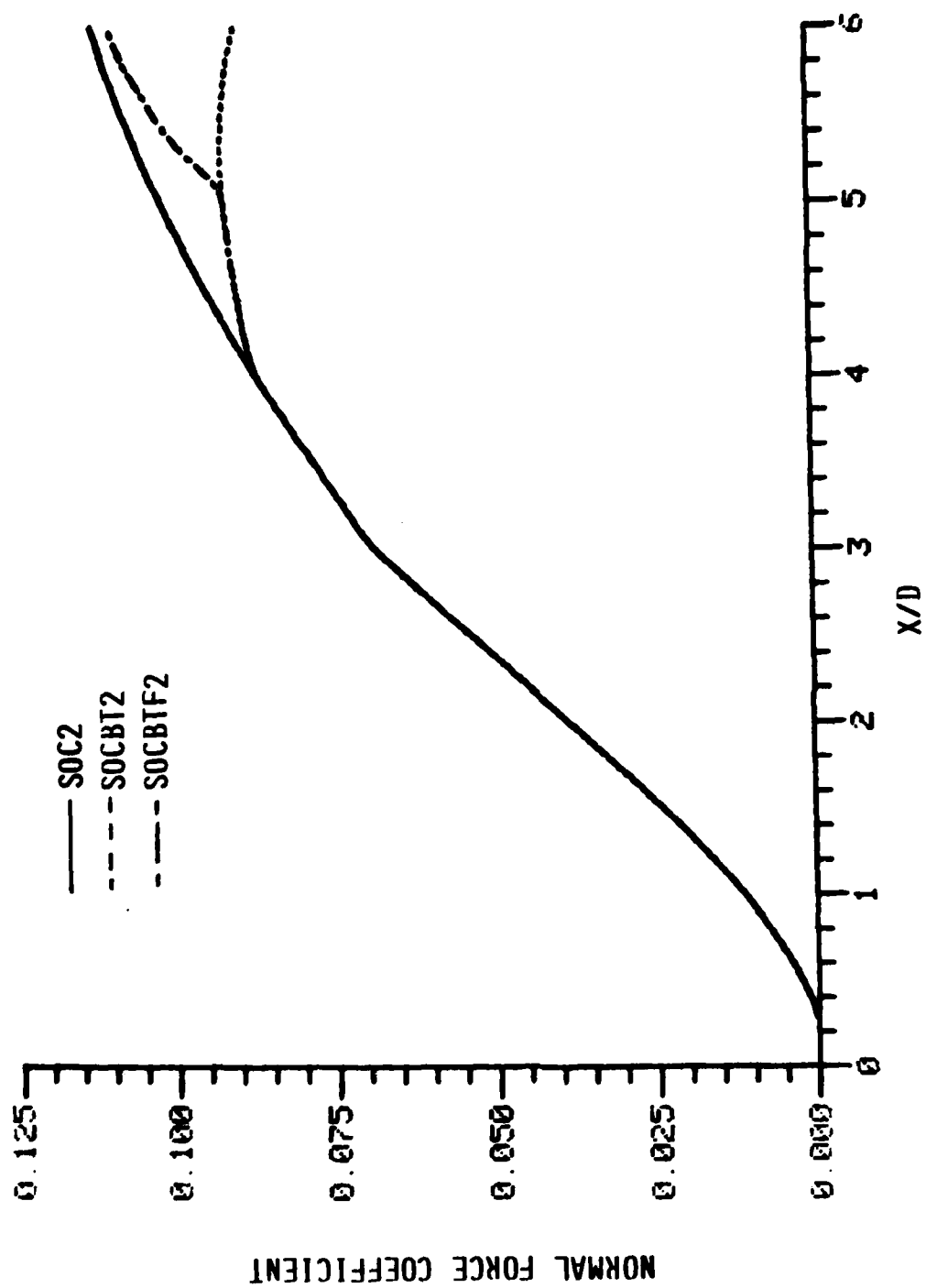
Figure 6. Continued

c. Mach = 4

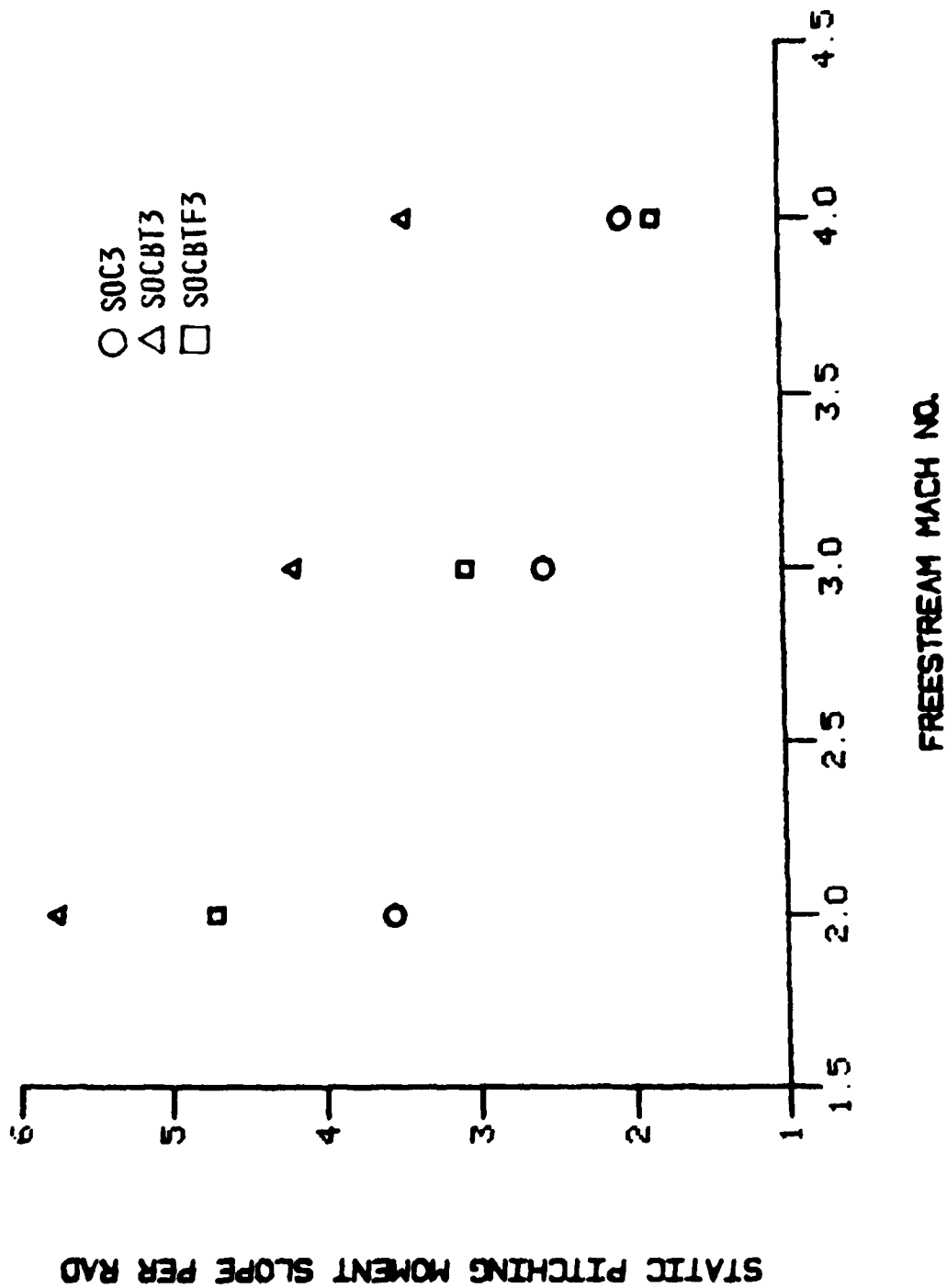FREESTREAM MACH NO.

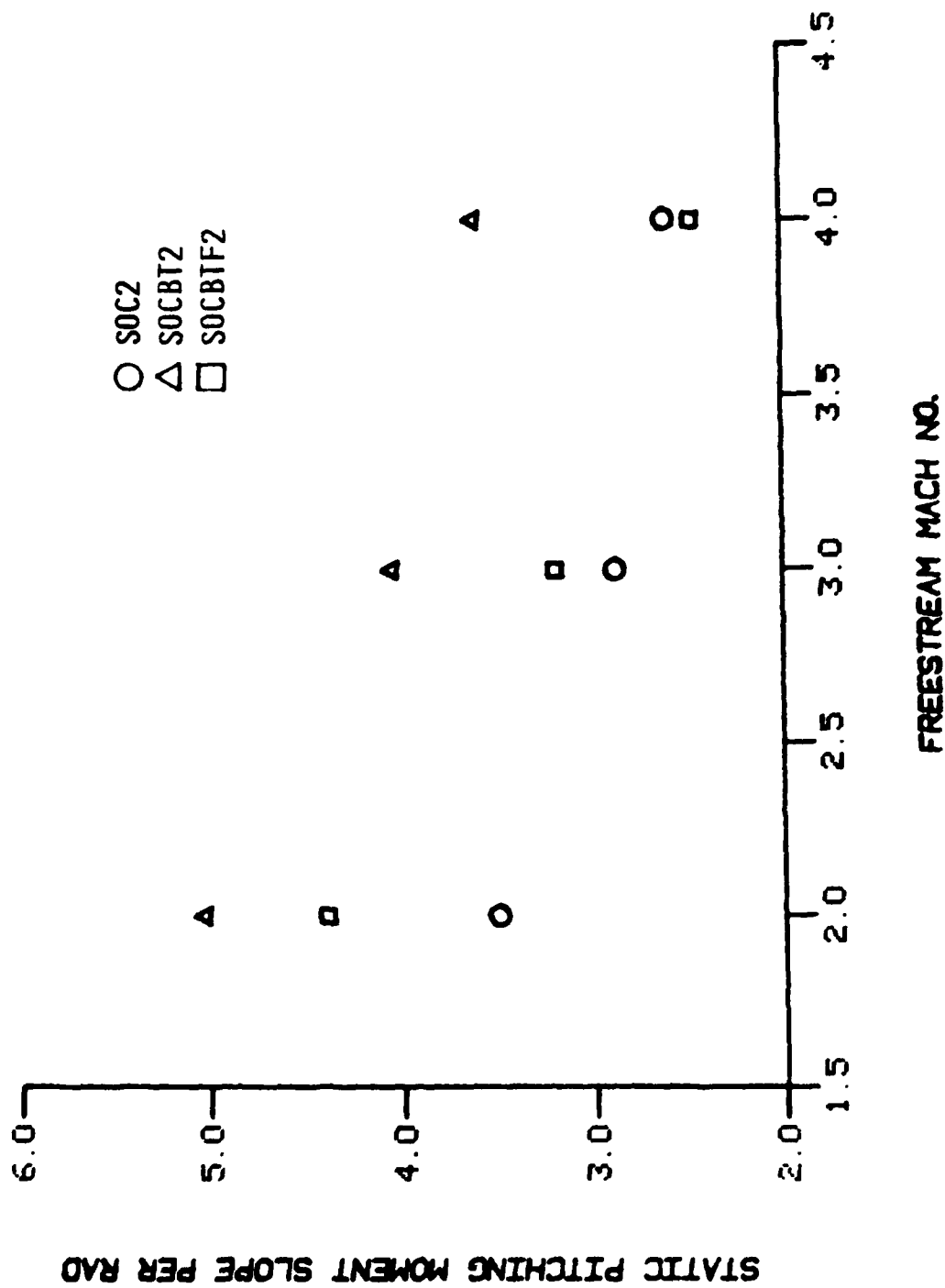Figure 7. Static Pitching Moment vs. Mach No.

a. SOC3, SOCBT3, SOCBTF3
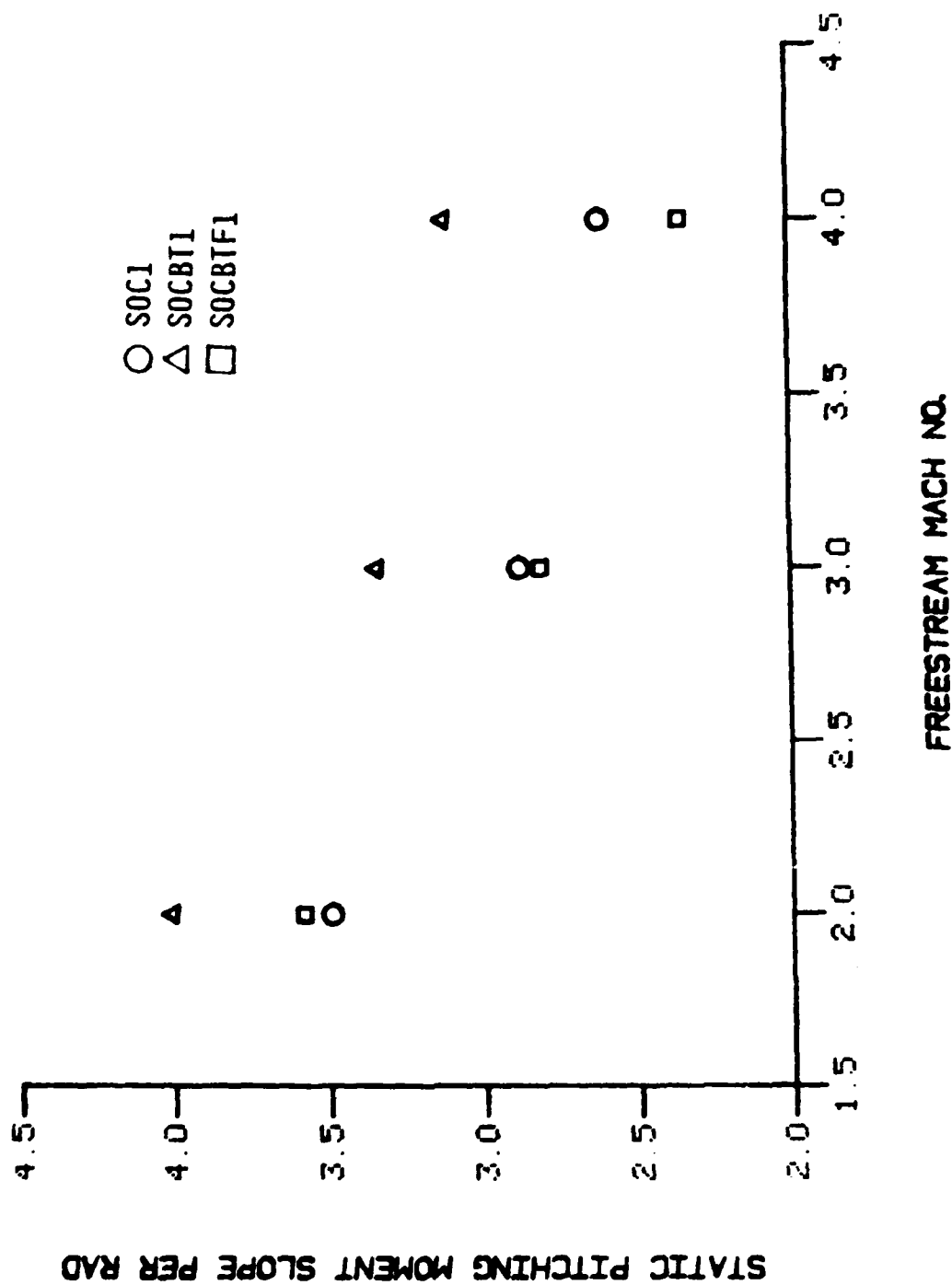
31

Figure 7. Continued

b. SOC2, SOCBT2, SOCBTF2

FREESTREAM MACH NO.

STATIC PITCHING MOMENT SLOPE PER RAD

○ SOC2
△ SOCBT2
□ SOCBTF2

1.5 2.0 2.5 3.0 3.5 4.0 4.5

2.0 3.0 4.0 5.0 6.0

32

FREESTREAM MACH NO.

Figure 7. Continued

c. SOC1, SOCBT1, SOCBTF1

33

FREESTREAM MACH NO.

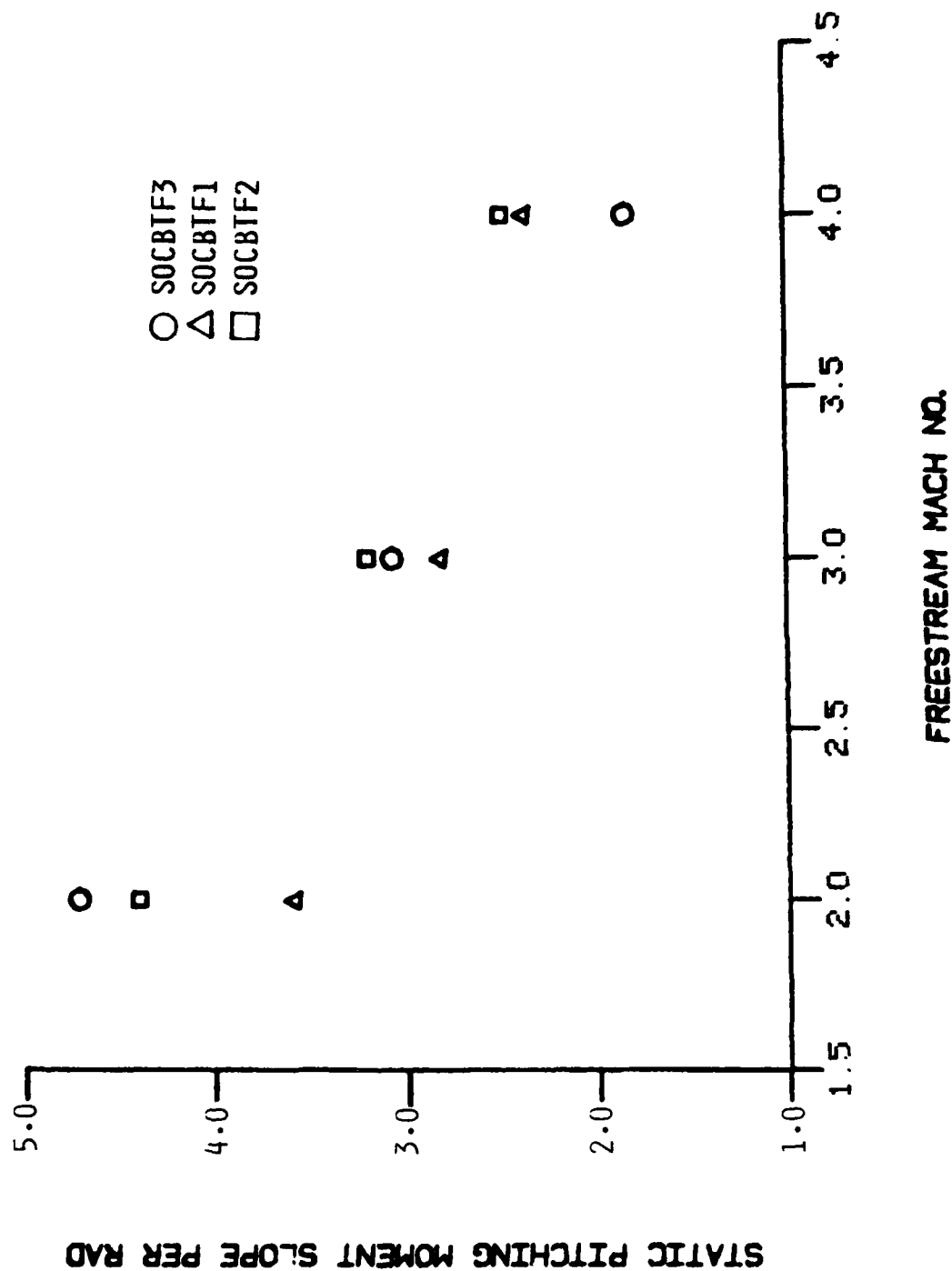STATIC PITCHING MOMENT SLOPE PER RAD
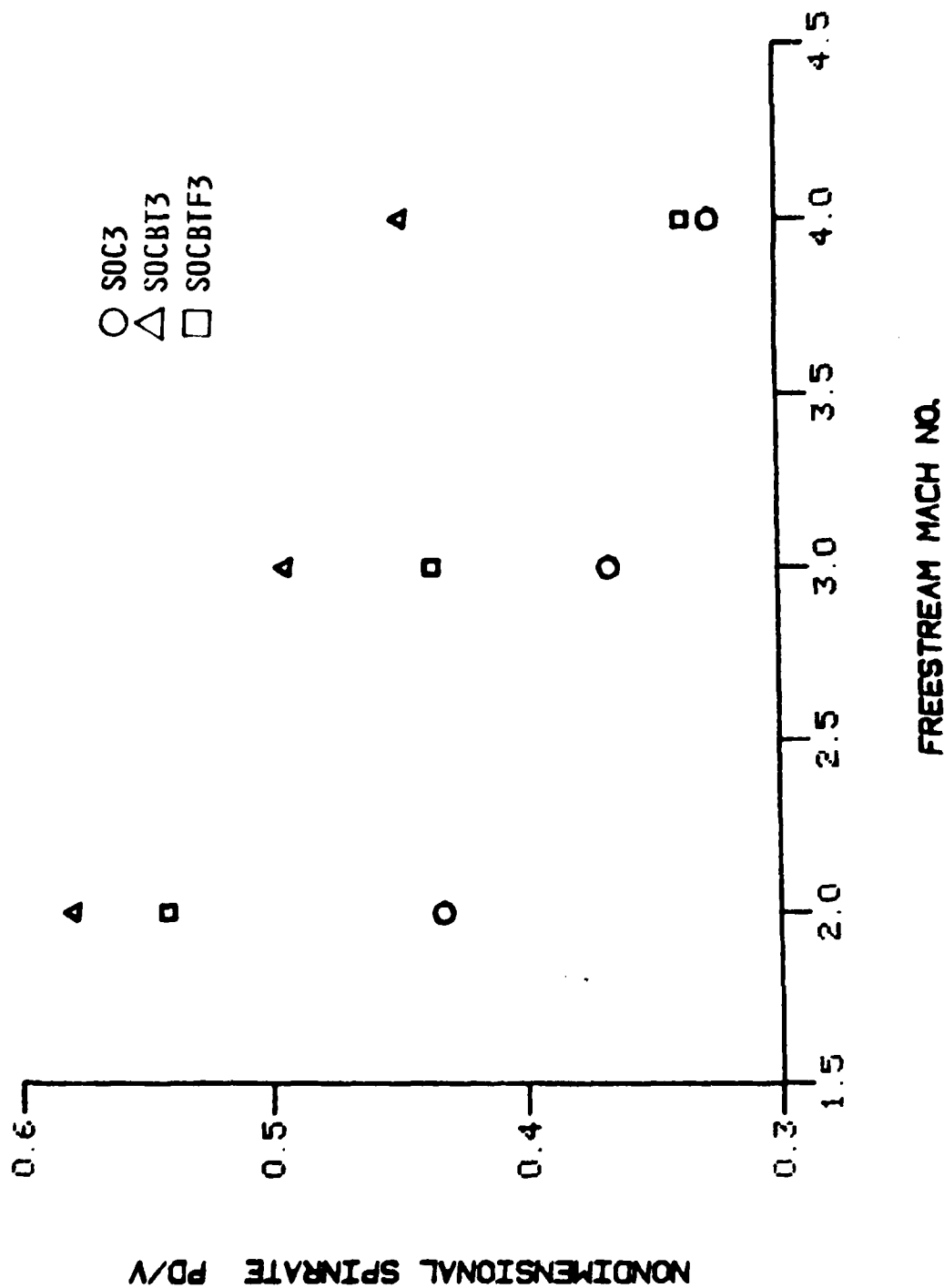
Figure 7. Continued

d. SOCBTF3, SOCBTF1, SOCBTF2

34

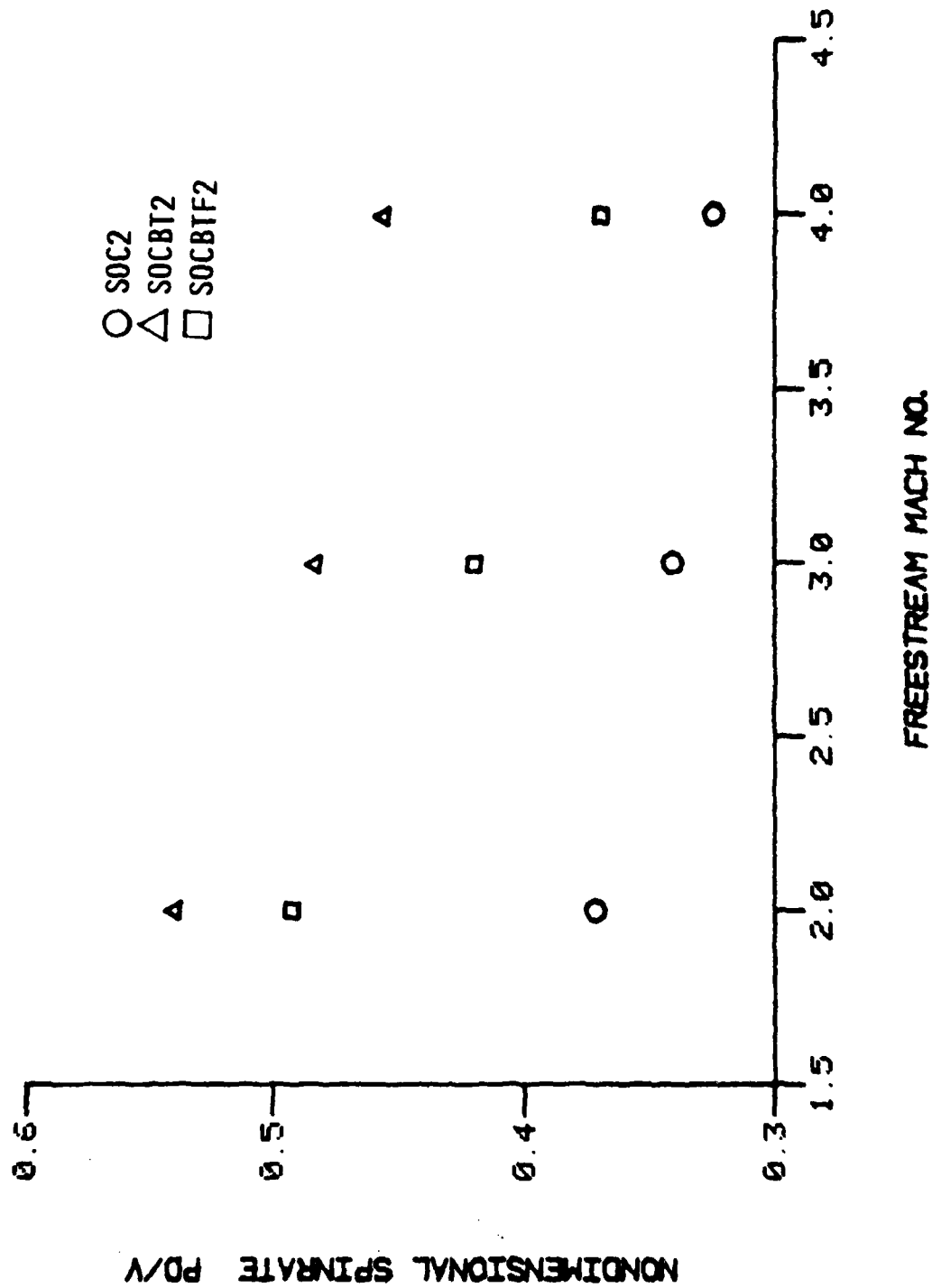Figure 8. Nondimensional Spinrate (pd/V) vs. Mach No., s_g = 1.3

a. SOC3, SOCBT3, SOCBTF3

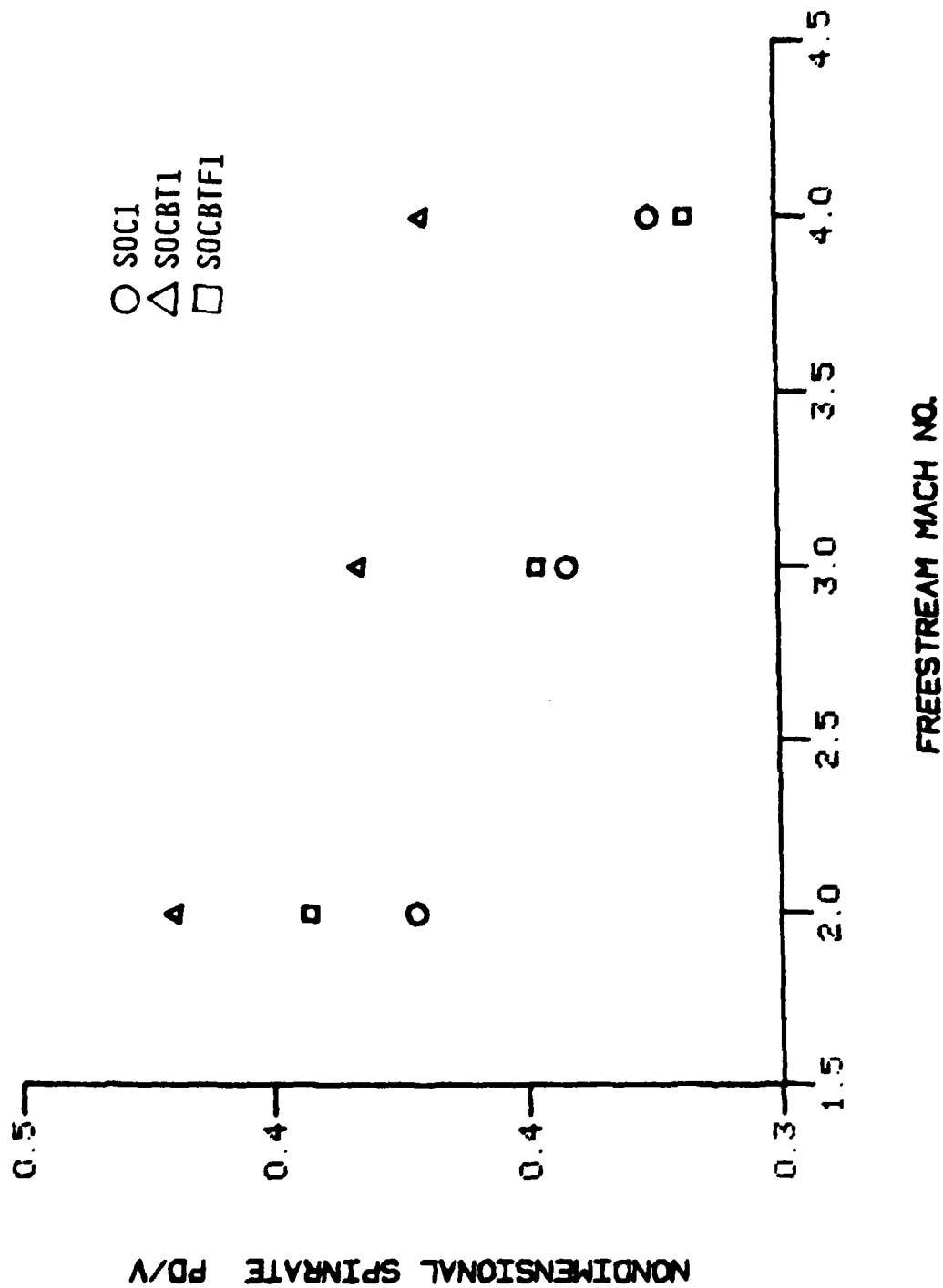Figure 8. Continued

b. SOC2, SOCBT2, SOCBTF2

Figure 8. Continued

c. SOC1, SOCBT1, SOCBTF1

FREESTREAM MACH NO.

Figure 8. Continued

d. SOCBTF3, SOCBTF1, SOCBTF2

FREESTREAM MACH NO.

DRAG COEFFICIENT

○ SOC3
△ SOCBT3
□ SOCBTF3
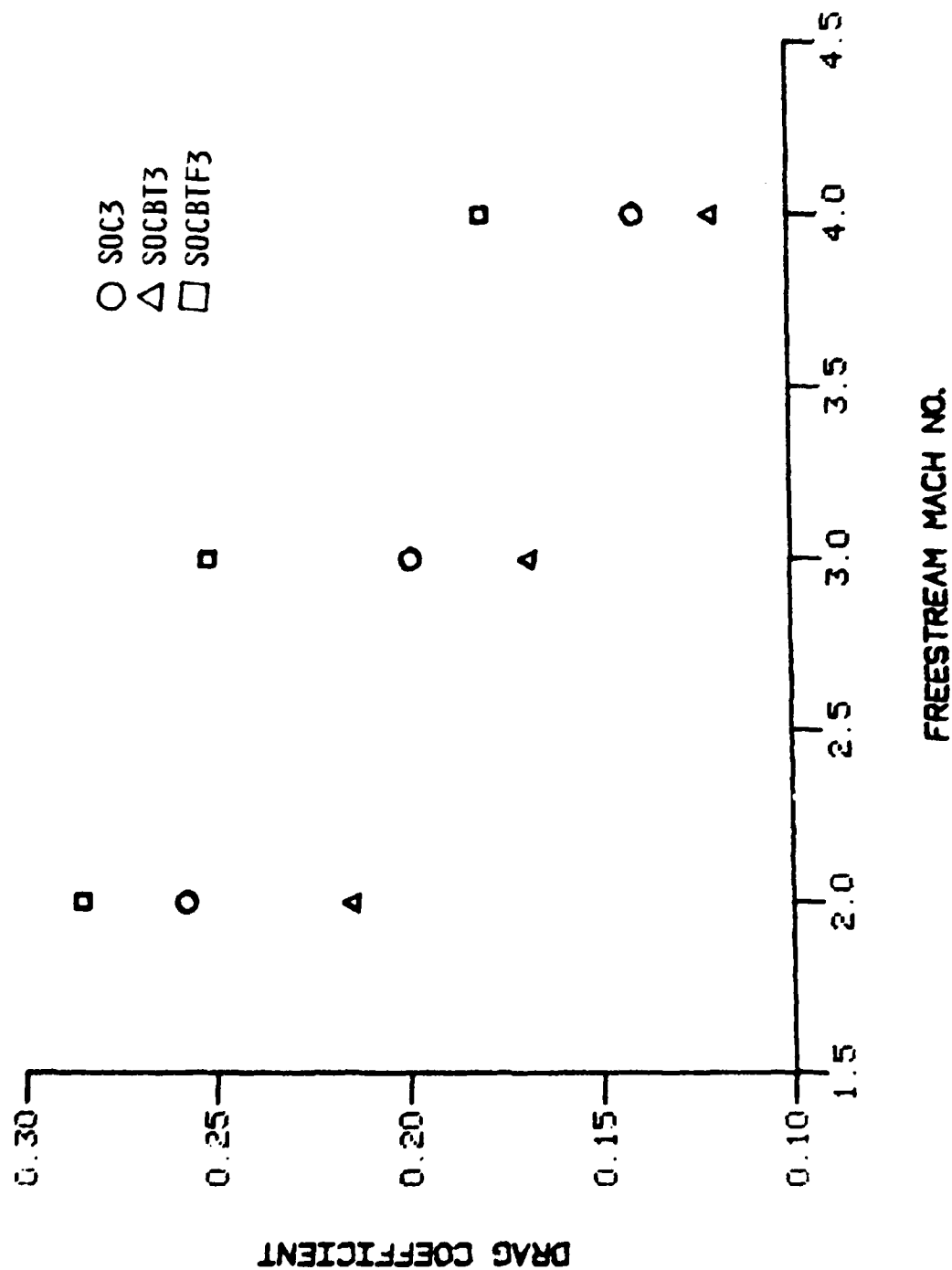
Figure 9. Drag Force Coefficient vs. Mach No.

a. SOC3, SOCBT3, SOCBTF3

FREESTREAM MACH NO.

Figure 9. Continued

b. SOC2, SOCBT2, SOCBTF2

FREESTREAM MACH NO.
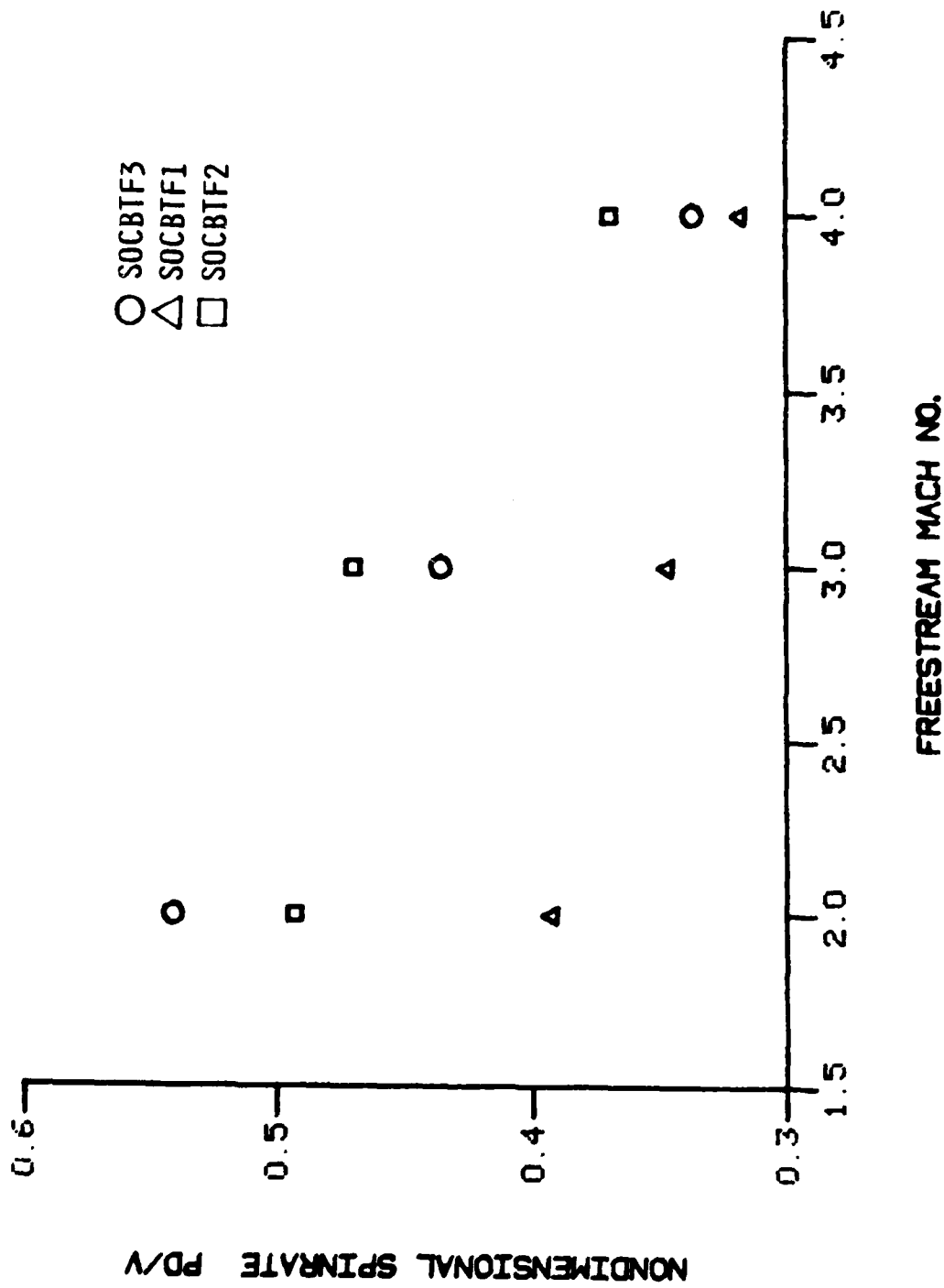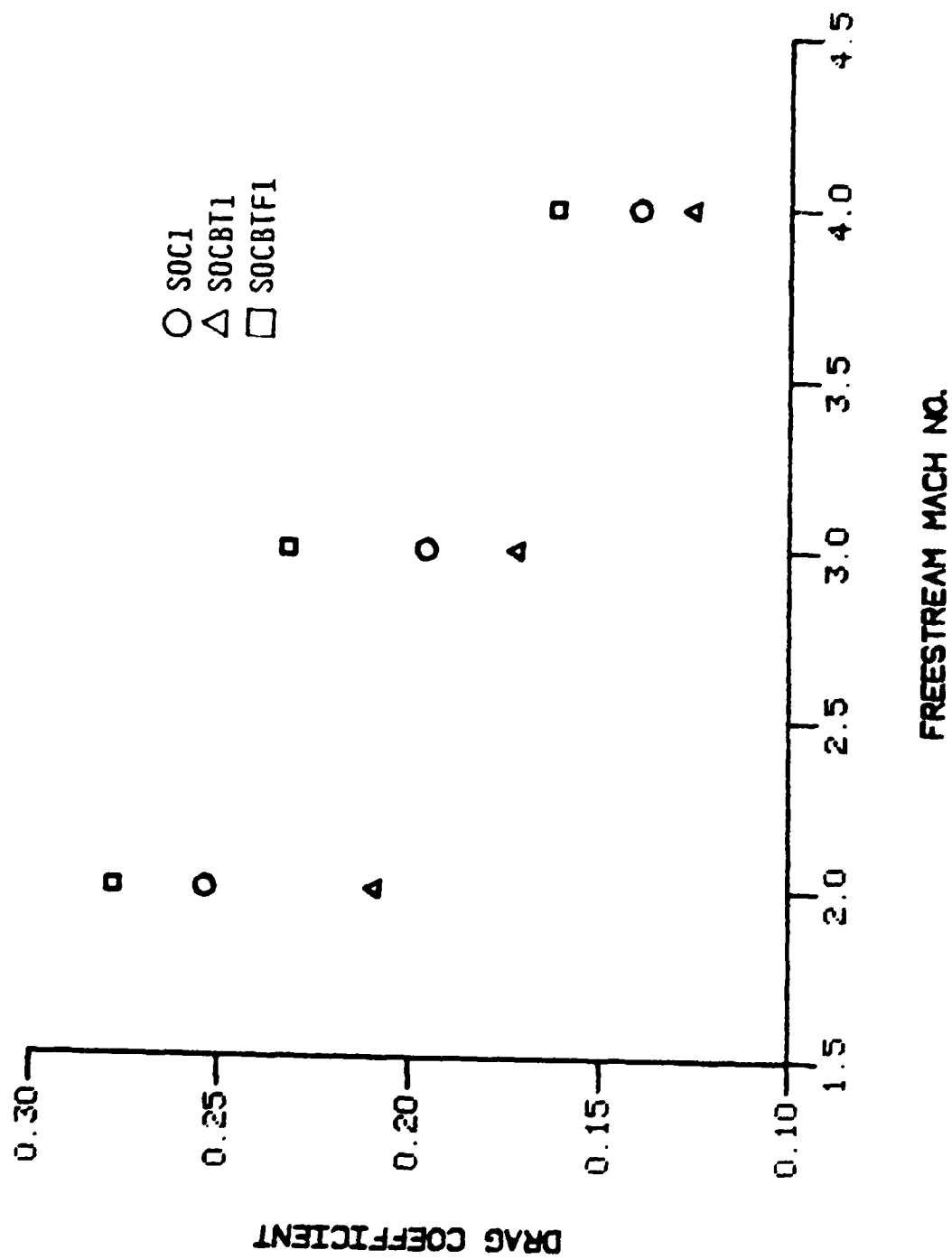
Figure 9. Continued

c. SOC1, SOCBT1, SOCBTF1
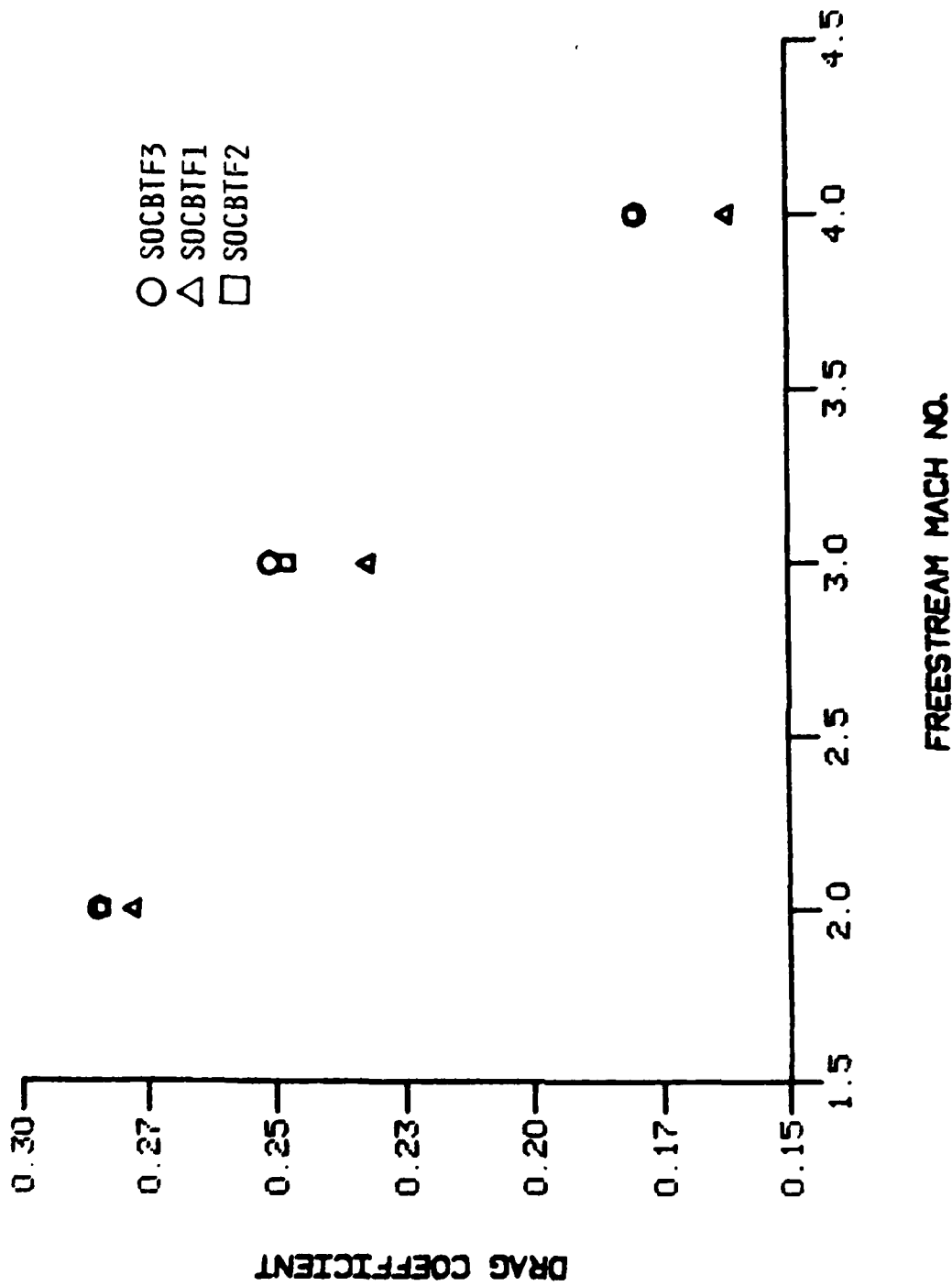
Figure 9. Continued

d. SOCBTF3, SOCBTF1, SOCBTF2
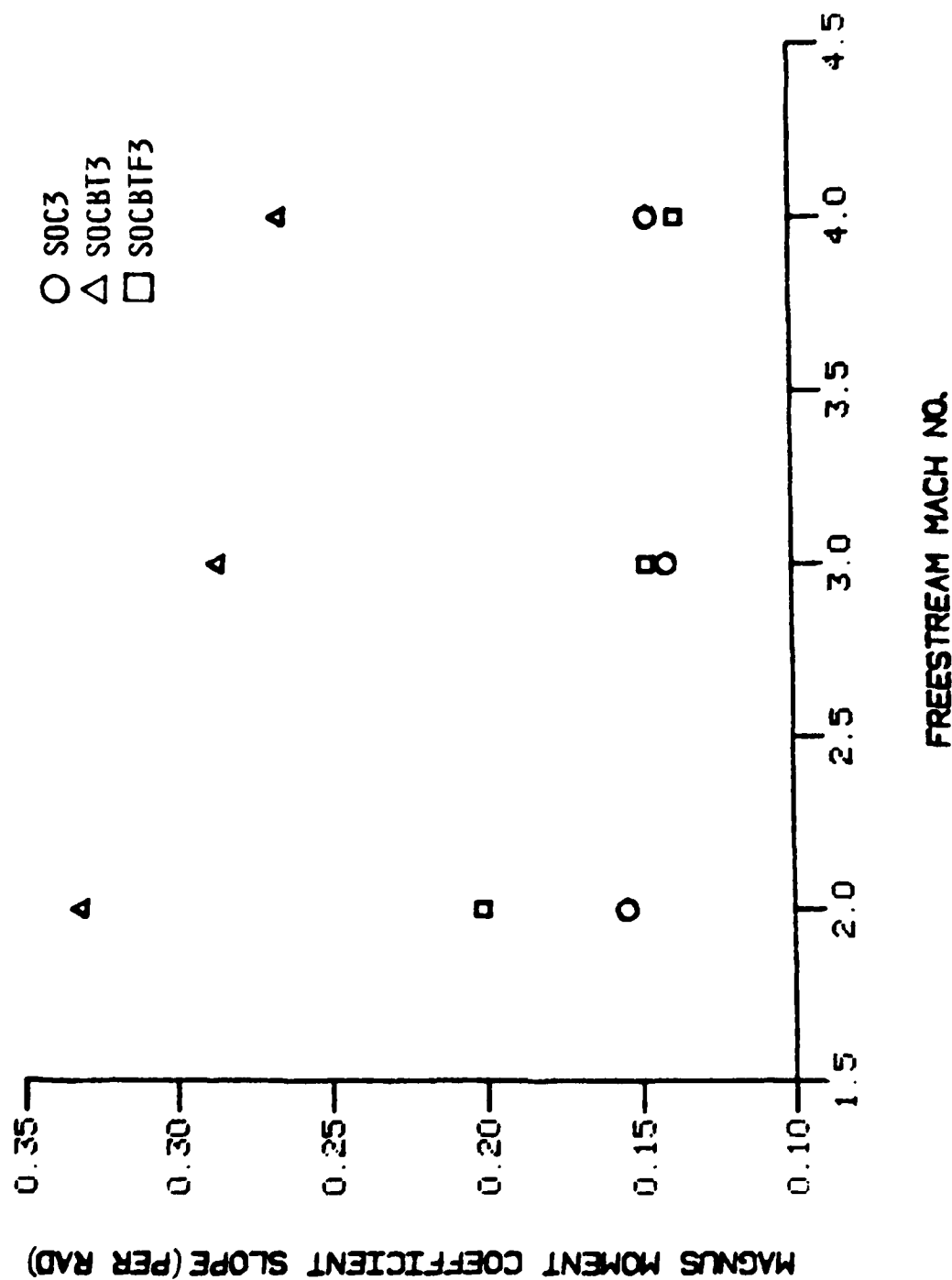
Figure 10. Magnus Moment Slope vs. Mach No.
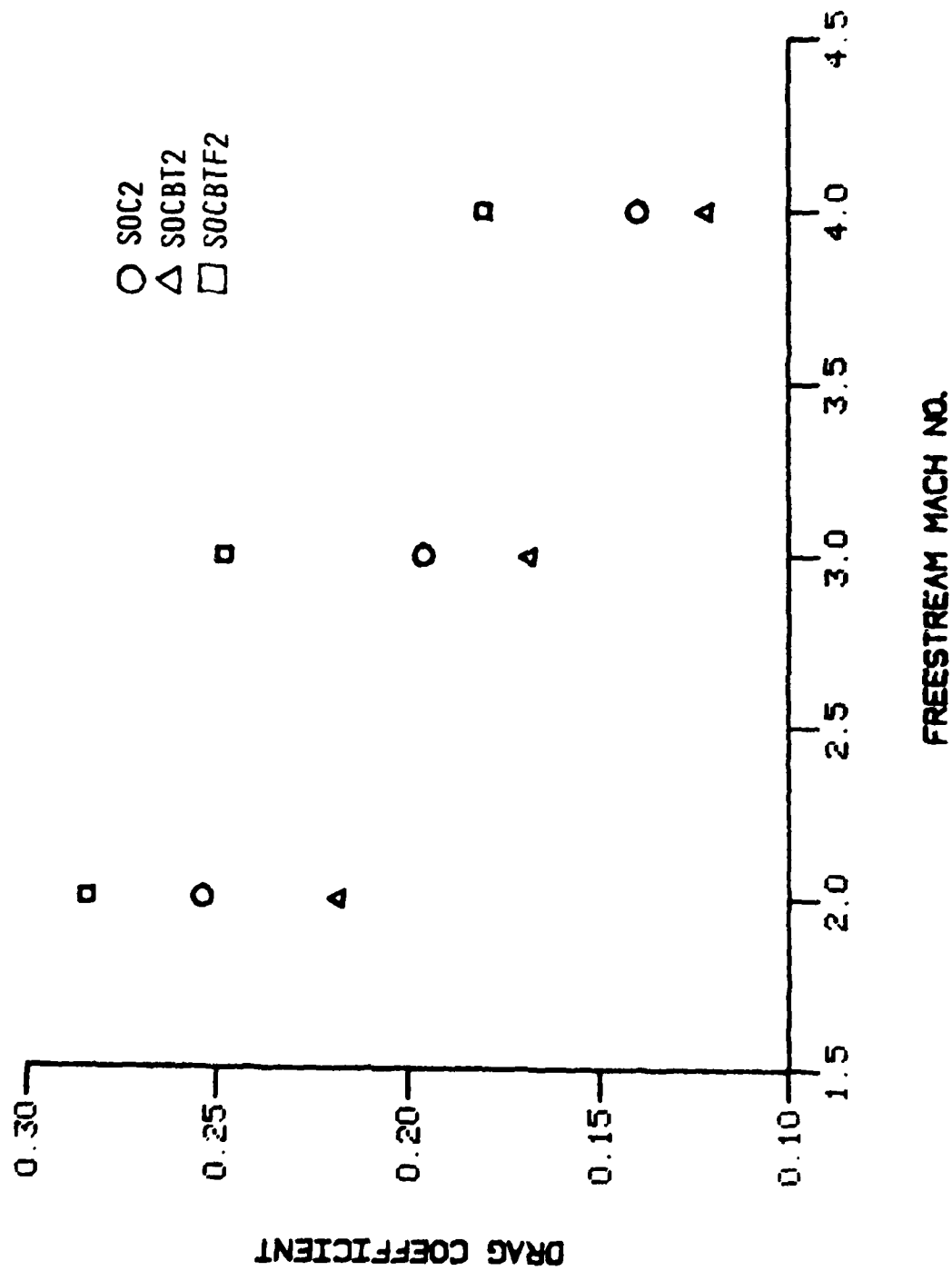
a. SOC3, SOCBT3, SOCBTF3
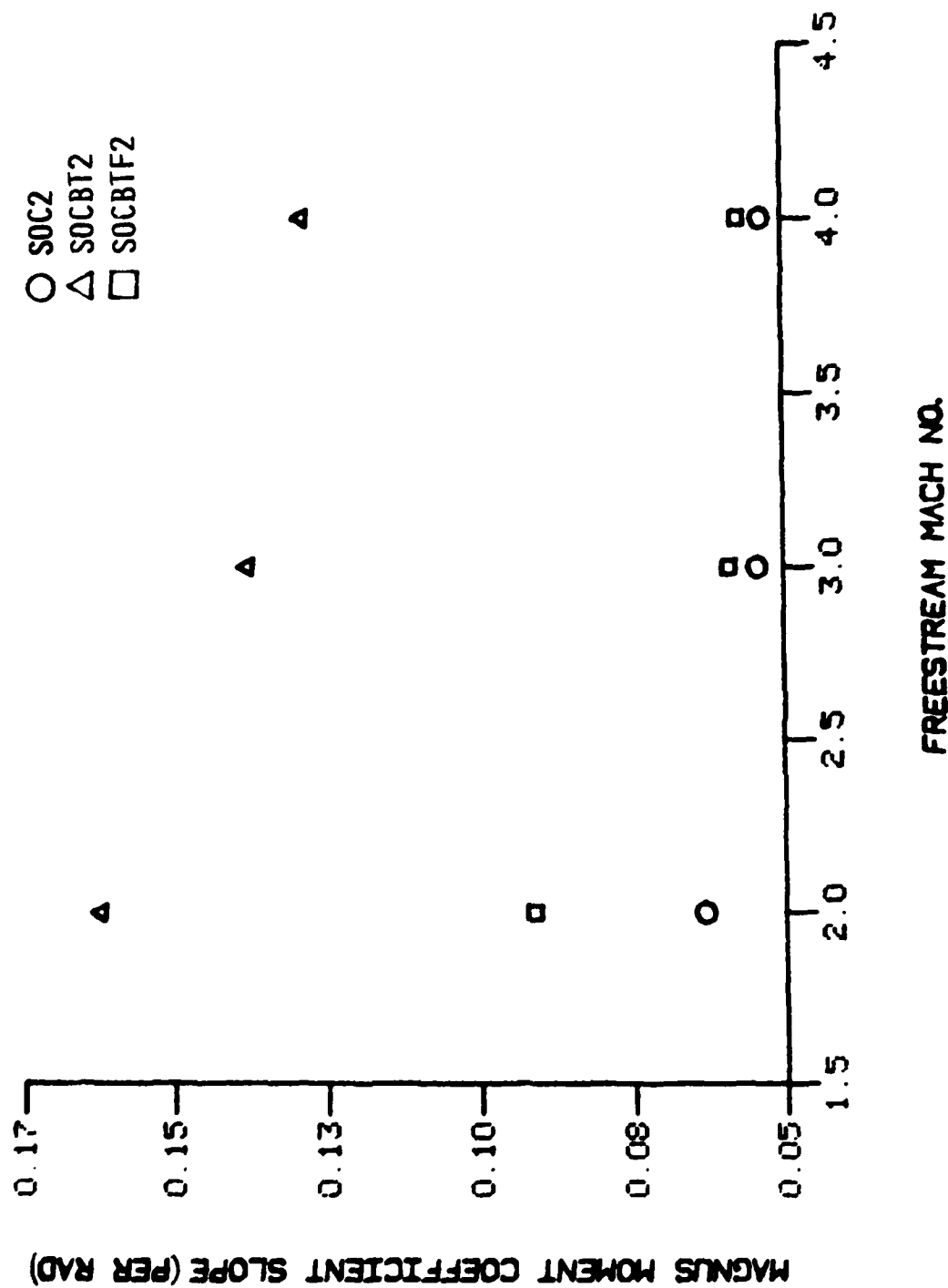
Figure 10. Continued

b. SOC2, SOCBT2, SOCBTF2

44

FREESTREAM MACH NO.
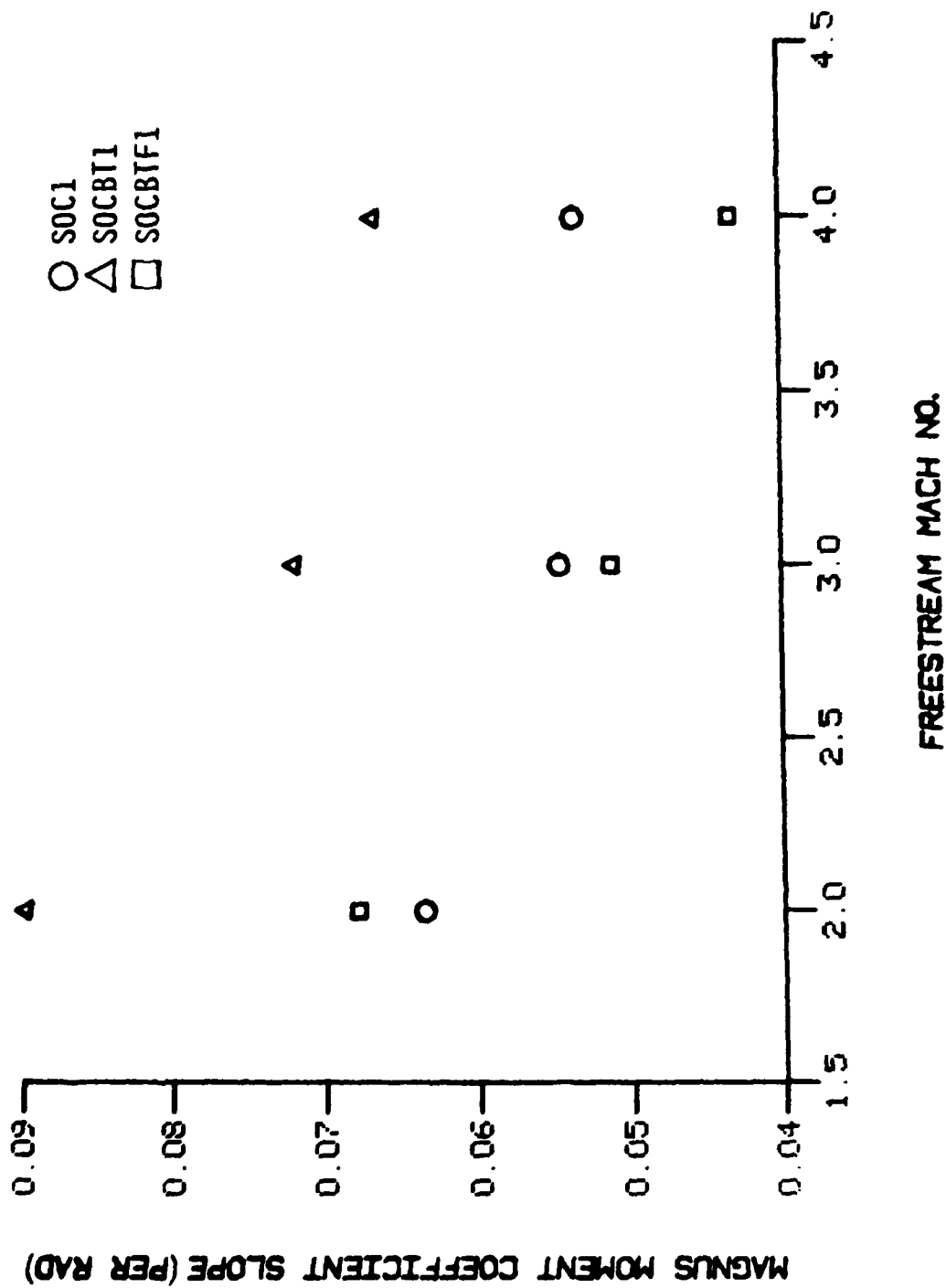
Figure 10. Continued

c. SOC1, SOCBT1, SOCBTF1,

45

FREESTREAM MACH NO.
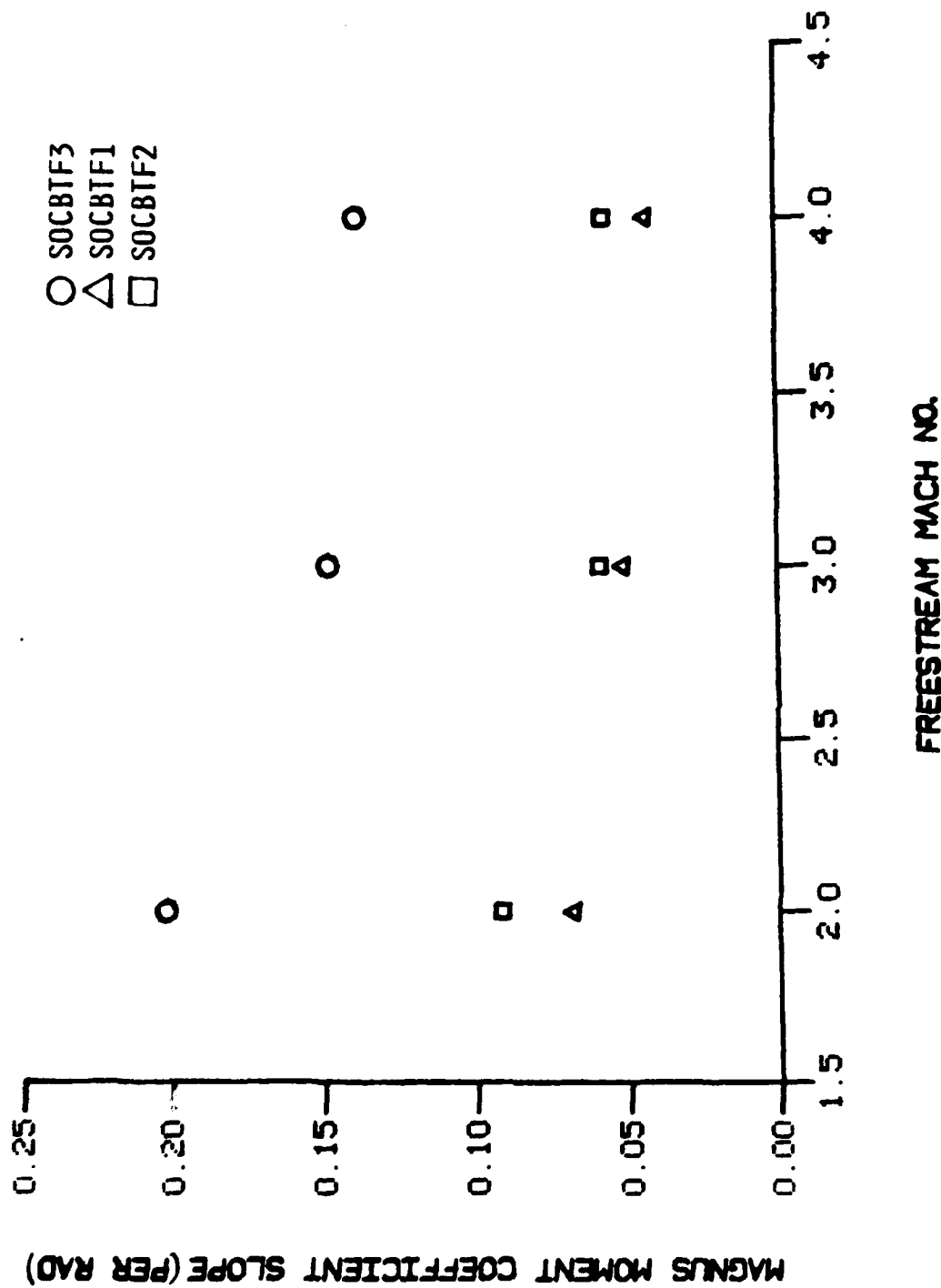
Figure 10. Continued

d. SOCBTF3, SOCBTF1, SOCBTF2

46
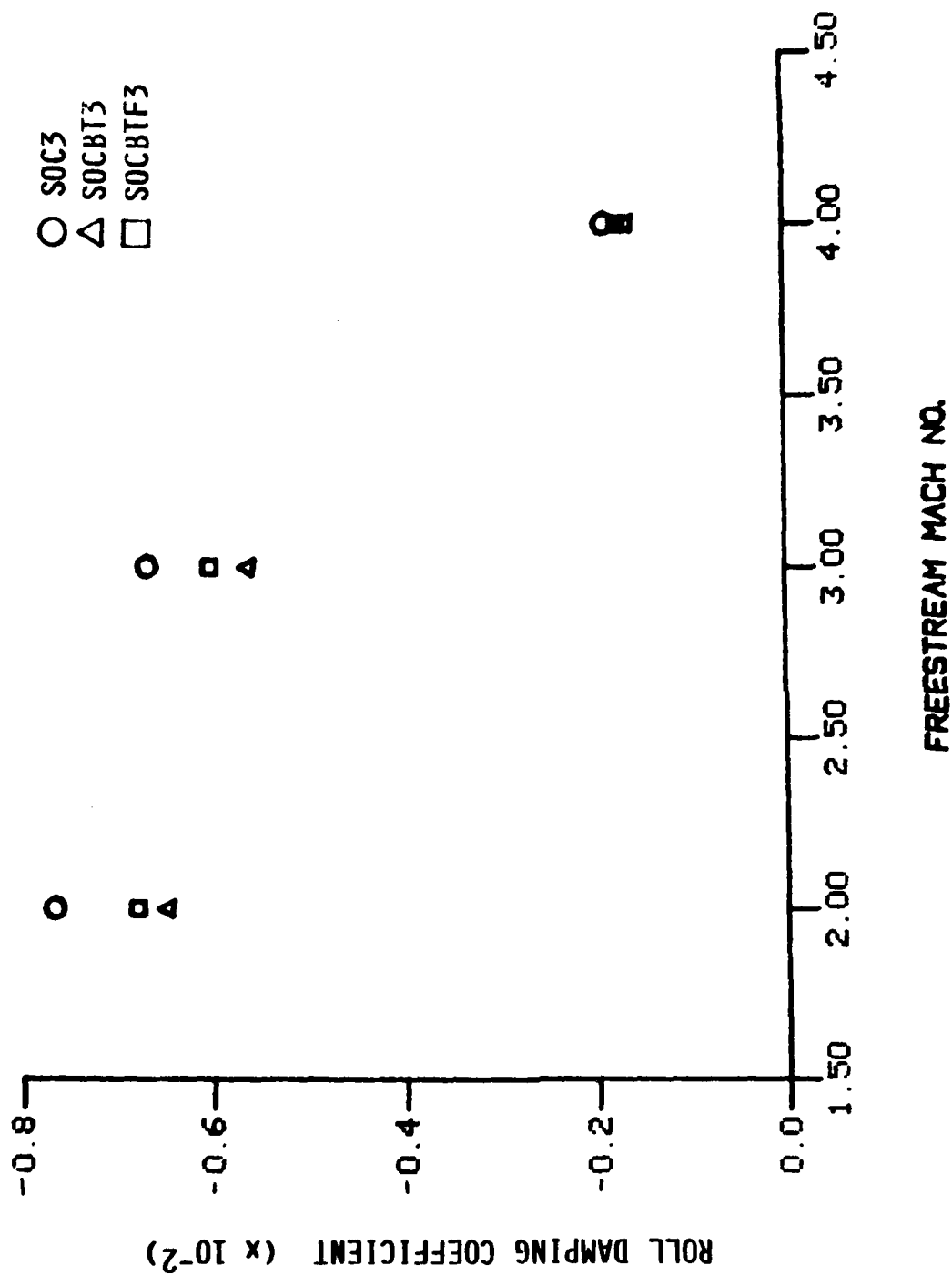
Figure 11. Roll Damping Coefficient vs. Mach No.

a. SOC3, SOCBT3, SOCBTF3

FREESTREAM MACH NO.
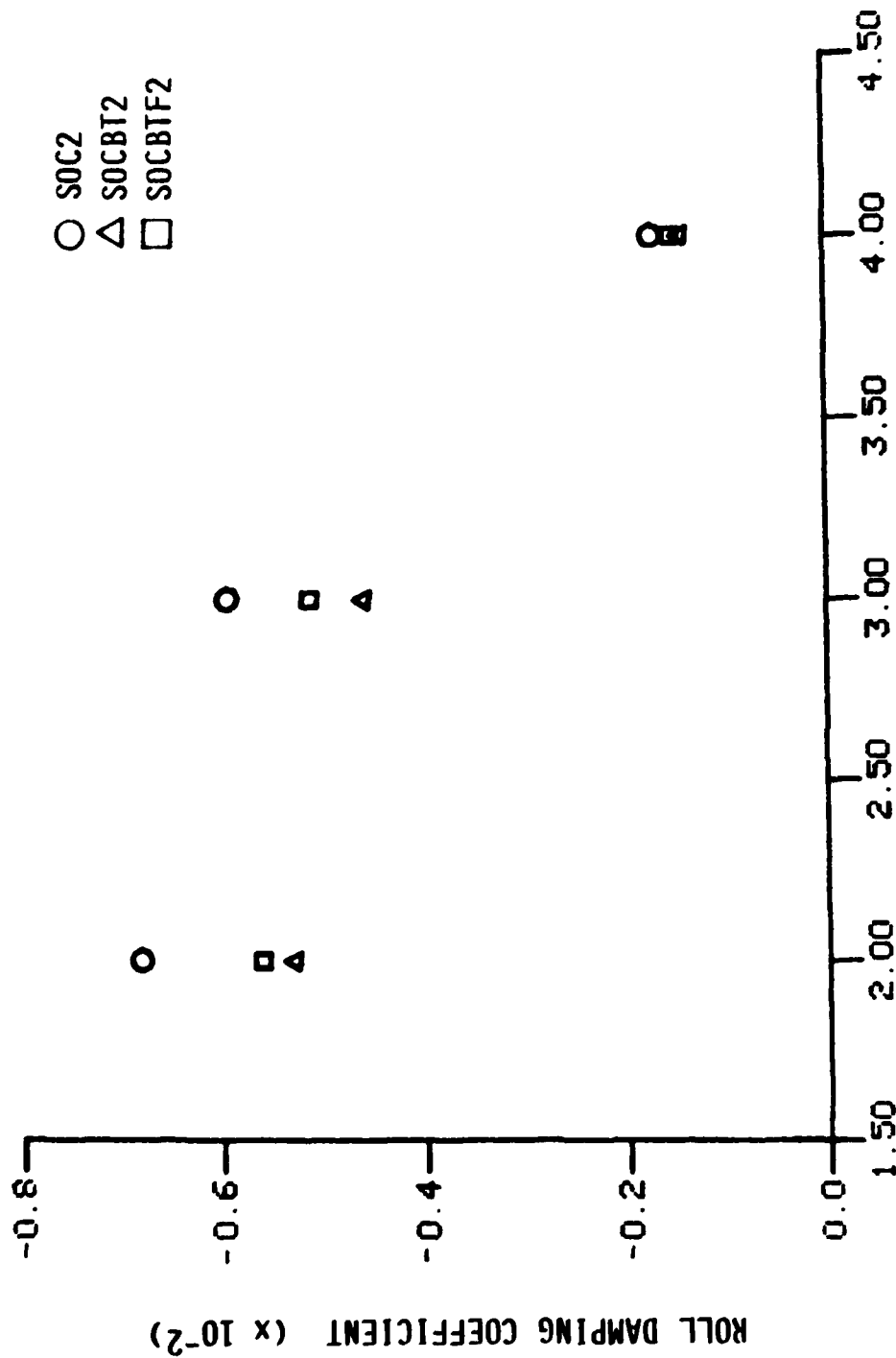
Figure 11. Continued

b. SOC2, SOCBT2, SOCBTF2
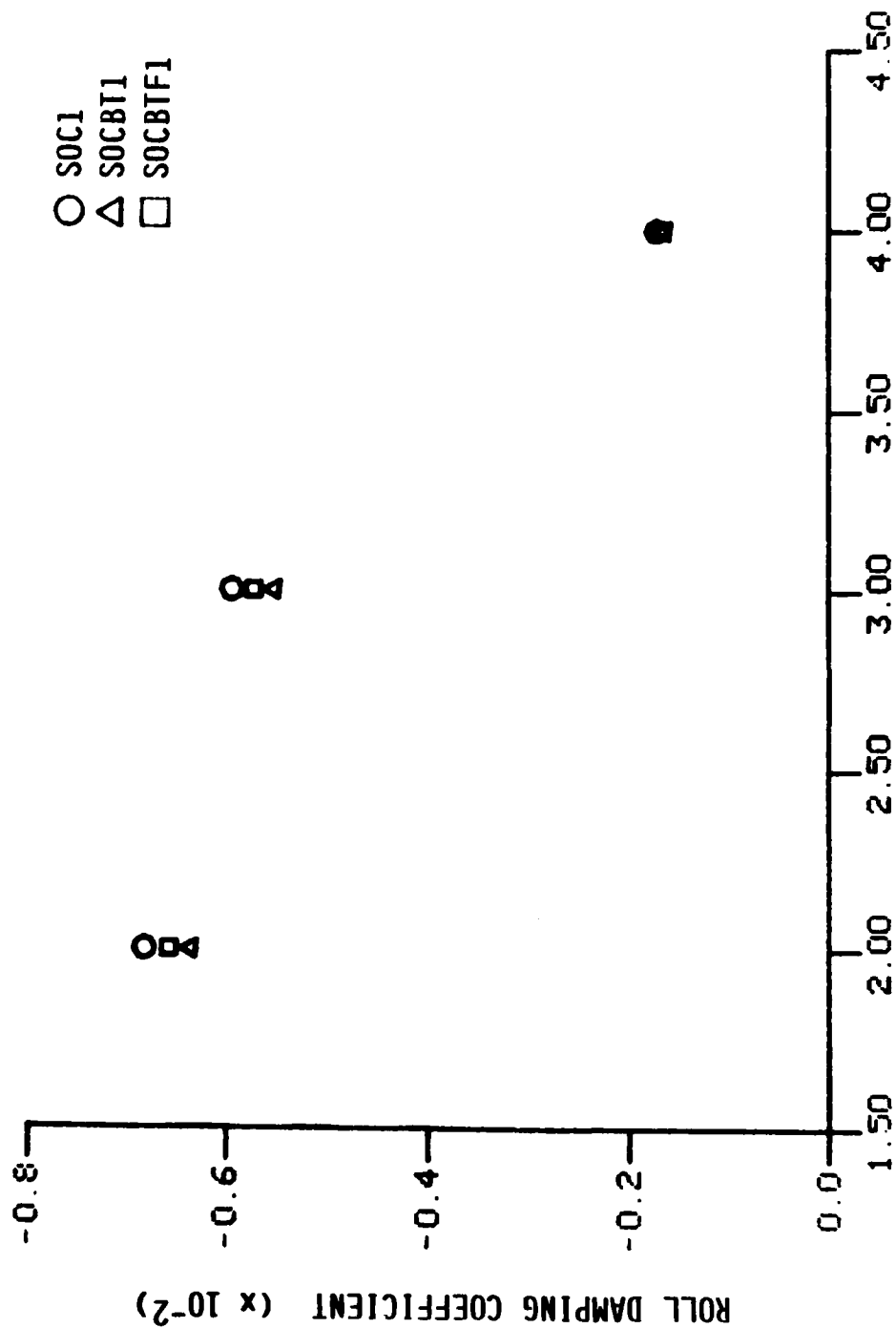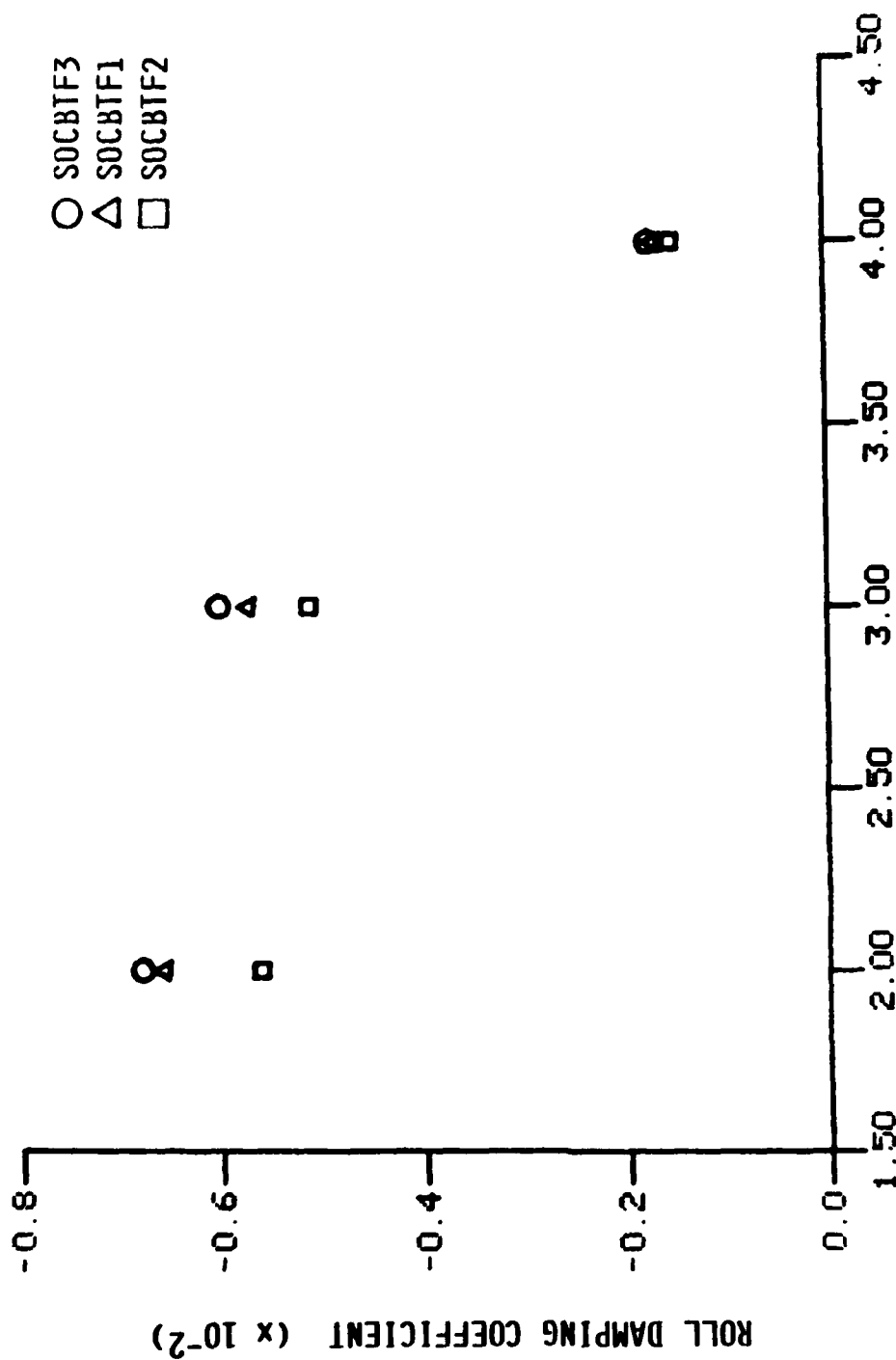
FREESTREAM MACH NO.

Figure 11. Continued

c. SOC1, SOCBT1, SOCBTF1

49

FREESTREAM MACH NO.

Figure 11. Continued

d. SOCBTF3, SOCBTF1, SOCBTF2

50

Figure 11. Continued

c. SOC1, SOCBT1, SOCBTF1

FREESTREAM MACH NO.
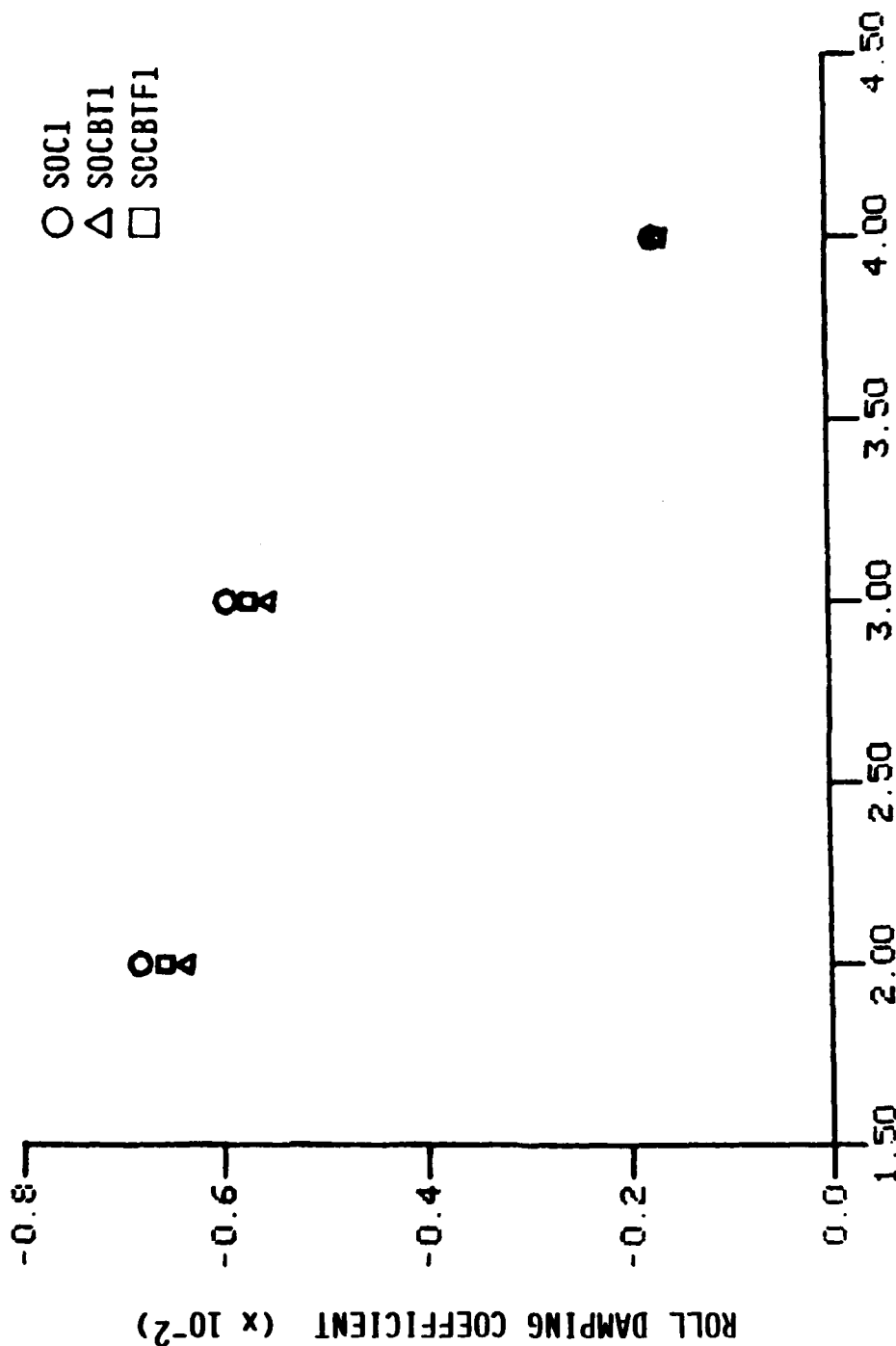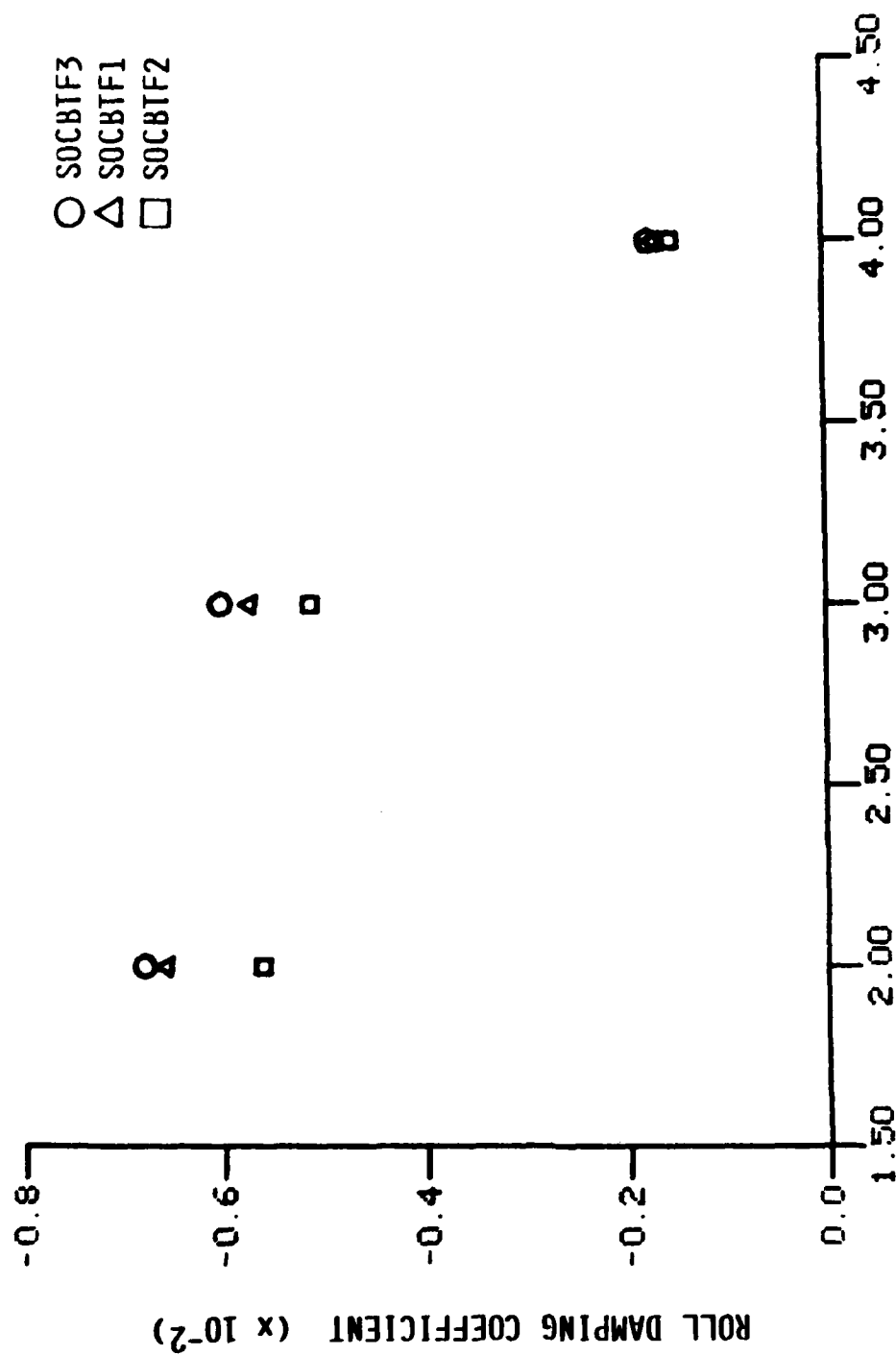
Figure 11. Continued

d. SOCBTF3, SOCBTF1, SOCBTF2

REFERENCES

1. Murphy, C.H., "Free Flight Motion of Symmetric Missiles," U.S. Army Ballistic Research Laboratory Report No. 1216, Aberdeen Proving Ground, Maryland 21005, July 1963 (AD 442757).

2. "Engineering Design Handbook - Design for Control of Projectile Flight Characteristics," Headquarters, US Army Materiel Command, September 1966.

3. Schiff, L.B., and Steger, J.L., "Numerical Simulation of Steady Supersonic Viscous Flow," AIAA Journal, Vol. 18, No. 12, December 1980, pp. 1421-1430.

4. Schiff, L.B., and Sturek, W.B., "Numerical Simulation of Steady Supersonic Flow Over an Ogive-Cylinder-Boattail Body," ARBRL-TR-02363, US Army Ballistic Research Laboratory, Aberdeen Proving Ground, Maryland 21005, September 1981 (AD A106060).

5. Sturek, W.B., and Schiff, L.B., "Computations of the Magnus Effect for Slender Bodies in Supersonic Flow," ARBRL-TR-02384, US Army Ballistic Research Laboratory, Aberdeen Proving Ground, Maryland 21005, December 1981 (AD A110016).

6. Sturek, W.B., and Mylin, D.C. "Computational Study of the Magnus Effect on Boattailed Shell," AIAA Journal, Vol. 20, No. 10, October 1982, pp. 1462-1464.

7. Sturek, W.B., Guidos, B., and Nietubicz, C.J., "Navier-Stokes Computational Study of the Influence of Shell Geometry on the Magnus Effect at Supersonic Speeds," ARBRL-TR-02501, US Army Ballistic Research Laboratory, Aberdeen Proving Ground, Maryland 21005, June 1983 (AD A130630).

8. Mueller, T.J., and Kayser L.D., "A Method of Determining the Turbulent Base Pressure in Uniform and Non-Uniform Supersonic Flows," ARBRL-TR-02374, US Army Ballistic Research Laboratory, Aberdeen Proving Ground, Maryland 21005, October 1981 (AD A107318).

9. Devan, L., and Mason, L.A., "Aerodynamics of Tactical Weapons to Mach Number 8 and Angle of Attack 180°: Part II, Computer Program and Users Guide," N.S.W.C. TR 81-358, September 1981.

10. McCoy, R.L., "McDrag - A Computer Program for Estimating the Drag Coefficients of Projectiles," ARBRL-TR-02293, US Army Ballistic Research Laboratory, Aberdeen Proving Ground, Maryland 21005, Febuary 1981 (AD A098110).

11. Robinson, M.L., "Boundary Layer Effects in Supersonic Flow over Cylinder-Flare Bodies," Australian Defense Scientific Service Weapons Research Establishment Report No. 1238, July 1974.

12. Platou, A.S., "The Influence of the Magnus Moment on the Dynamic Stability of a Projectile," ARBRL-MR-2155, US Army Ballistic Research Laboratory, Aberdeen Proving Ground, Maryland 21005, January 1972 (AD 738016).

LIST OF SYMBOLS

C_D	=	drag coefficient
C_{DB}	=	base drag coefficient (Equation 4)
C_{ℓ_p}	=	roll damping coefficient
C_{M_α}	=	slope of static pitching moment coefficient
$C_{m_{p\alpha}}$	=	slope of Magnus moment coefficient
$C_{M_q} + C_{M\dot{\alpha}}$	=	pitch damping coefficient
C_{N_α}	=	slope of normal force coefficient
d	=	maximum body diameter, m
I_x	=	axial moment of inertia, kg - m^3
I_y	=	transverse moment of inertia, kg - m^3
k_x	=	axial radius of gyration
k_y	=	transverse radius of gyration
L1	=	cylindrical body length
L2	=	boattail afterbody length
L3	=	flare afterbody length
M_∞	=	freestream Mach number
p	=	axial angular velocity, rad/sec
P_B/P_∞	=	ratio of base pressure to freestream pressure
pd/V	=	nondimensional spinrate about projectile axis
s_g	=	gyroscopic stability factor (Equation 1)
s_d	=	dynamic stability factor (Equation 2)
V	=	air speed, m/sec
X/D	=	projectile length in calibers
γ	=	ratio of specific heats
ρ	=	air density, kg/m^3

DISTRIBUTION LIST

No. of Copies	Organization	No. of Copies	Organization
12	Administrator Defense Technical Info Center ATTN: DTIC-DDA Cameron Station Alexandria, VA 22314	1	Director US Army Air Mobility Research and Development Laboratory Ames Research Center Moffett Field, CA 94035
1	Commander US Army Materiel Development and Readiness Command ATTN: DRCDMD-ST 5001 Eisenhower Avenue Alexandria, VA 22333	1	Commander US Army Communications Research and Development Command ATTN: DRSEL-ATDD Fort Monmouth, NJ 07703
9	Commander Armament Research and Development Center US Army Armament, Munitions and Chemical Command ATTN: DRSMC-TDC (D) DRSMC-TSS (D) DRSMC-LCA-F (D) Mr. D. Mertz Mr. E. Falkowski Mr. A. Loeb Mr. R. Kline Mr. S. Kahn Mr. H. Hudgins Dover, NJ 07801	1	Commander US Army Electronics Research and Development Command Technical Support Activity ATTN: DELSD-L Fort Monmouth, NJ 07703
		2	Commander US Army Missile Command ATTN: DRSMI-R DRSMI-RDK Mr. R. Deep Redstone Arsenal, AL 35898
1	Commander US Army Armament, Munitions and Chemical Command ATTN: DRSMC-LEP-L (R) Rock Island, IL 61299	1	Commander US Army Missile Command ATTN: DRSMI-YDL Redstone Arsenal, AL 35898
1	Director Armament Research and Development Center Benet Weapons Laboratory US Army Armament, Munitions and Chemical Command ATTN: DRSMC-LCB-TL(D) Watervliet, NY 12189	1	Commander US Army Tank Automotive Command ATTN: DRSTA-TSL Warren, MI 48090
		1	Director US Army TRADOC Systems Analysis Activity ATTN: ATAA-SL White Sands Missile Range NM 88002
1	Commander US Army Aviation Research and Development Command ATTN: DRDAV-E 4300 Goodfellow Blvd. St. Louis, MO 63120	1	Commander US Army Research Office P. O. Box 12211 Research Triangle Park NC 27709

55

DISTRIBUTION LIST

No. of Copies	Organization	No. of Copies	Organization
1	Commander US Naval Air Systems Command ATTN: AIR-604 Washington, D. C. 20360	1	ACUREX Corporation/Aerotherm ATTN: Dr. M. J. Abbett 485 Clyde Avenue Mountain View, CA 94042

2	Commander
	David W. Taylor Naval Ship
	  Research and Development
	  Center
	ATTN: Dr. S. de los Santos
	      Mr. Stanley Gottlieb
	Bethesda, Maryland 20084
		1	Bendix Guided Systems Division
			ATTN: MS 2/17A (S. Wasserman)
			Teterboro, NJ 97608

2	Commander
	US Naval Surface Weapons Center
	ATTN: Dr. F. Moore
	      Mr. P. Daniels
	Dahlgren, VA 22448
		1	Nielsen Engineering &
			  Research, Inc.
			ATTN: Dr. S. Stahara
			510 Clyde Avenue
			Mountain View, CA 94043

4	Commander
	US Naval Surface Weapons Center
	ATTN: Code K24
	      Dr. W. Yanta
	      Code R44
	      Dr. C. Hsieh
	      Dr. T. Zien
	      Dr. R. U. Jettmar
	Silver Spring, MD 20910
		2	Sandia Laboratories
			ATTN: Technical Staff,
			        Dr. W.L. Oberkampf
			        Aeroballistics Division
			        5631, H.R. Vaughn
			Albuquerque, NM 87115

		1	Massachusetts Institute of Technology ATTN: Tech Library 77 Massachusetts Avenue Cambridge, MA 02139
1	Commander US Naval Weapons Center ATTN: Code 3431, Tech Lib China Lake, CA 93555	1	University of Delaware Mechanical and Aerospace Engineering Department ATTN: Dr. J. E. Danberg Newark, DE 19711

1	Director
	NASA Langley Research Center
	ATTN: NS-185, Tech Lib
	Langley Station
	Hampton, VA 23365
			Aberdeen Proving Ground
			
			Dir, USAMSAA
			  ATTN: DRXSY-D
			         DRXSY-MP, H. Cohen

2	Commandant
	US Army Infantry School
	ATTN: ATSH-CD-CSO-OR
	Fort Benning, GA 31905
			Cdr, USATECOM
			  ATTN: DRSTE-TO-F
			
			Cdr, CRDC, AMCCOM
			  ATTN: DRSMC-CLB-PA

1	AFWL/SUL Kirtland AFB, NM 87117		DRSMC-CLN DRSMC-CLJ-L DRSMC-CLB-PA (Mr. M.C. Miller)

USER EVALUATION OF REPORT

Please take a few minutes to answer the questions below; tear out
this sheet, fold as indicated, staple or tape closed, and place
in the mail. Your comments will provide us with information for
improving future reports.

1. BRL Report Number_____

2. Does this report satisfy a need? (Comment on purpose, related
project, or other area of interest for which report will be used.)

_____

_____

_____

3. How, specifically, is the report being used? (Information
source, design data or procedure, management procedure, source of
ideas, etc.)_____

_____

_____

4. Has the information in this report led to any quantitative
savings as far as man-hours/contract dollars saved, operating costs
avoided, efficiencies achieved, etc.? If so, please elaborate.

_____

_____

5. General Comments (Indicate what you think should be changed to
make this report and future reports of this type more responsive
to your needs, more usable, improve readability, etc.)_____

_____

_____

_____

6. If you would like to be contacted by the personnel who prepared
this report to raise specific questions or discuss the topic,
please fill in the following information.

                    Name:_____

          Telephone Number:_____

Organization Address:_____

                        _____

                        _____